

Experiments 32a and 32b

COMPTON SCATTERING

INTRODUCTION	1
THEORY	2
Characteristics of Compton scattering	2
Kinematics: the Compton scattering formula (Experiment 32a)	3
Dynamics: the Klein-Nishina formula (Experiment 32b)	5
Scattering cross section	5
Klein-Nishina scattering cross section	6
THE APPARATUS	8
Overview: capturing Compton events	8
Pulse processing electronics	10
Software	12
MCA application	12
Compton Experiment application	13
Interpreting scatter plots	15
EXPERIMENT 32A	17
Purpose of the experiment	17
Procedure	17
Detector calibrations	17
Compton scattering energy vs. angle data collection	18
Securing the experiment	19
Analysis	19
Data analysis Mathematica® notebook	20
Optional investigation	21
Prelab Problems	22
EXPERIMENT 32B	23
Purpose of the experiment	23
Procedure	23
Electronics setup	23
Geometry measurements	23
Compton scattering rate vs. angle data collection	24
Securing the experiment	24
Analysis	25
Overview	25
Solid angle captured by the detected events	25

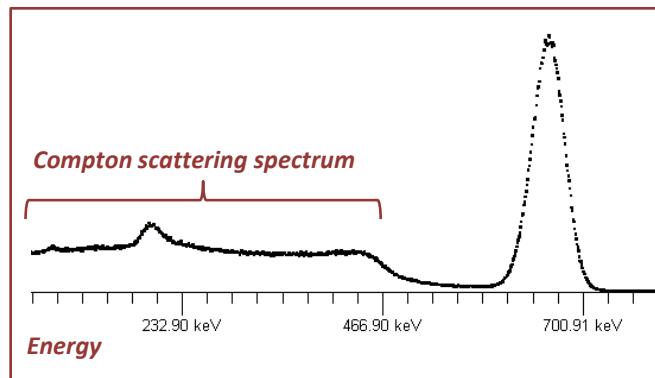
Nal detector efficiency corrections	26
Target scintillator self-absorption and multiple scattering corrections	27
Mitigating the effect of multiple scatterings in the target	28
Putting it all together	29
Prelab Problems	30
APPENDIX A: TOTAL AND DIFFERENTIAL SCATTERING CROSS SECTIONS	1
Total scattering cross section and the mean free path	1
Differential scattering cross section	3
APPENDIX B: THOMSON SCATTERING AND ITS RELATIVISTIC COUNTERPART	1
Thomson scattering	1
Relativistic, single photon scattering	4
Electron spin, pair production	7
APPENDIX C: MASS ATTENUATION COEFFICIENTS	1
Summary Data	1
Charts	2

COMPTON SCATTERING

INTRODUCTION

Experiment 30a introduced you to *Compton scattering* of high-energy photons by electrons. Your scintillator spectra acquired during that experiment included evidence of many Compton scattering events, as in Figure 1. A scintillator Compton spectrum shows the range of kinetic energies of the outgoing electrons following their interactions with the gamma ray photons. Experiments 32a and 32b more thoroughly investigate this interesting phenomenon, first predicted and then experimentally verified by the American physicist Arthur Compton.¹

Figure 1: A portion of a NaI scintillator spectrum of the energies deposited by 0.66MeV gamma ray photons emitted by a ^{137}Cs source. The Compton spectrum is clearly visible.



In Experiment 32a the *kinematics* of Compton scattering are thoroughly investigated using γ -ray photons emitted by a ^{137}Cs source. By considering the photon-electron interaction as an elastic collision between two particles, the outgoing energies of the scattered photon and recoiling electron are compared to the Compton scattering formula, derivable from a simple calculation using special relativity. Experiment 32b delves more deeply into the phenomenon by investigating the interaction *dynamics*: the electromagnetic forces exerted by the photon on the electron determine their probabilities of scattering into various angles. The *Klein-Nishina scattering formula* is a quantum-theoretical prediction of these probabilities.² The instrumentation used for these experiments is a very small scale version of what is commonly used for high-energy particle research.

¹ Arthur Holly Compton won the 1927 Nobel Prize for his 1923 experiments. Compton demonstrated the particulate nature of electromagnetic radiation, first theorized by Einstein in his 1905 explanation of the photoelectric effect (for which Einstein won the 1921 Nobel Prize). Compton was a famous and important figure in American physics research, even appearing on the cover of *Time Magazine* in 1936.

² The Swedish physicist Oskar Klein and the Japanese physicist Yoshio Nishina jointly derived their famous formula in 1928 while working with Niels Bohr in Copenhagen, Denmark. Read more about their achievement in the Theory section below and in this text's Appendix B.

THEORY

Characteristics of Compton scattering

One must be careful to distinguish Compton scattering from other processes for scattering electromagnetic radiation by matter. The defining characteristic of Compton scattering is that it is a *quantum* process associated with an *incoherent interaction* between a single photon and a *free* electron. It is a quantum process because the incident electromagnetic radiation must be interpreted as a stream of photons (*quanta*), each behaving as an independent particle with kinetic energy and momentum.³

Compton scattering is *incoherent*: it is completely describable by considering the interaction of a single photon with a single electron, ignoring the fact that there may be many nearby “spectator” electrons (within a fraction of a nanometer, and whose wave functions may significantly overlap that of the target electron). In contrast, descriptions of phenomena such as metallic and specular reflections, refraction, and diffraction require *phase-coherent* interactions of the incident radiation with many electrons over distances large compared to the radiation’s wave length.

Compton scattering involves the response of a *free* (unbound) electron. Of course, atomic electrons are bound to their atoms by Coulomb forces. If, however, the energy of the photon-electron interaction is large compared to the electron’s binding energy to its parent atom, then that binding energy may offer only a small perturbation, and Compton scattering is a good model of the interaction. This will be most applicable to high-energy photons (x-rays and γ -rays) encountering weakly bound (valence) electrons, especially in light atoms such as carbon. At low photon energies, the binding energy of the electron must not be ignored. In the case of visible light, whose photon energies are small compared to even an outer electron’s binding energy, incoherent scattering by atomic electrons becomes *Rayleigh scattering*.⁴

³ Interestingly, this idea is in some sense a vindication of Rene Descartes’s and Isaac Newton’s *corpuscular theory* of light (c. 1670). Newton thought of light as composed of massless particles moving at finite velocity. His theory of light remained popular until the late 18th century, after which Christian Huygens’s wave theory finally took precedence. Turns out both theories were right, and therefore both were wrong! More correctly, both are thought to be different asymptotic limits of the more comprehensive theory called *quantum electrodynamics*, which is, in turn, now considered to be part of the low-energy asymptotic limit of *electroweak theory*, part of the standard model of particle physics.

⁴ After the British physicist J. W. Strutt (Lord Rayleigh, 1842–1919). Rayleigh scattering is an incoherent version of the atomic electrons’ responses which gives rise to *refraction* of visible light. It is mainly responsible for the blue color of the sky (in contrast, bodies of water more than a couple of meters deep appear blue mainly because of resonant absorption of long wavelengths by water molecules). Rayleigh was awarded the 1904 Nobel Prize in Physics for his discovery of argon (with the British chemist William Ramsay, who received the 1904 Prize in Chemistry).

Kinematics: the Compton scattering formula (Experiment 32a)

We shall analyze the kinematics of Compton scattering as an elastic collision between a photon and an electron (initially at rest) as shown in Figure 2. The derivation here is reproduced from the corresponding section of General Appendix A: *Relativistic Kinematics*.⁵ To simplify the notation, we choose units such that $c \equiv 1$ and $\hbar \equiv 1$. Thus both the photon's kinetic energy and its momentum may be represented by its wave number (in these units, its kinetic energy and its momentum are equal), and the electron's mass m is represented by its rest energy, 0.511 MeV. Given the incoming photon's energy k_0 and particle rest energy m , we want the outgoing photon energy k' as a function of its outgoing direction (turned by angle θ from the incoming photon trajectory); the particle's outgoing 4-momentum following the interaction is then (E_m, \vec{p}) .⁶

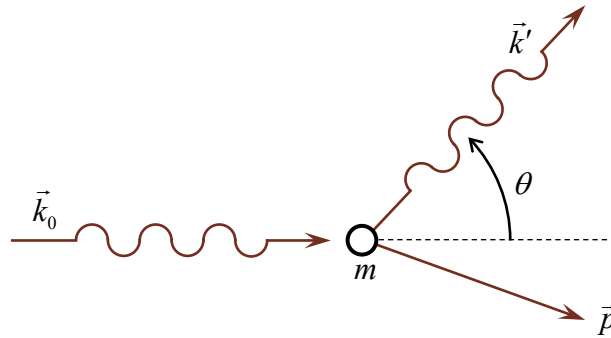


Figure 2: Compton scattering of a photon by an initially stationary electron.

Start with energy conservation: the total system energy is unaffected by the collision. Since the electron is an elementary particle, its rest mass must remain constant, and the collision must be elastic. Thus:

Energy conservation:

$$k_0 + m = k' + E_m$$

$$\therefore (k_0 + m - k')^2 = E_m^2 = p^2 + m^2$$

where in the second equation above we've used the relativistic invariance of the norm of the electron's 4-momentum, its rest energy: $m^2 = E_m^2 - p^2$. The outgoing electron's kinetic energy T is given by $T = E_m - m = k_0 - k'$. When $\theta = 180^\circ$, the corresponding electron kinetic energy T is called the *Compton edge energy*.

To continue the derivation, use momentum conservation to determine p^2 , which is the sum of the squares of its horizontal and vertical components in Figure 2. The vertical component equals

⁵ http://www.sophphx.caltech.edu/Physics_7/General_Appendix_A.pdf.

⁶ Recall that the relativistic *4-momentum* of an object has a time-like component equal its total energy and a space-like vector equal to its linear momentum vector. It has a Lorentz-invariant norm (time-like component squared minus the squared magnitude of the space-like vector) equal to square of the object's *rest energy* (internal energy).

that of the outgoing photon: $k' \sin \theta$; the horizontal component of p equals the difference between two photons' horizontal components: $k_0 - k' \cos \theta$. Therefore,

Momentum conservation:

$$\begin{aligned} p^2 &= (k_0 - k' \cos \theta)^2 + (k' \sin \theta)^2 \\ &= k_0^2 + k'^2 - 2k_0 k' \cos \theta \end{aligned}$$

Substituting this expression for p^2 into the energy conservation expression and collecting terms:

$$m(k_0 - k') = k_0 k' (1 - \cos \theta)$$

Solving for k' gives the important result:

Compton scattering formula

$$k' = \frac{k_0}{1 + \frac{k_0}{m}(1 - \cos \theta)} = \frac{k_0}{1 + 2 \frac{k_0}{m} \sin^2 \frac{1}{2} \theta} \quad (32.1)$$

This is the kinematic relationship between incoming and outgoing photon energies you will test in Experiment 32a. Compton expressed this relationship in terms of the photons' wavelengths:

$$\lambda' - \lambda_0 = \lambda_c (1 - \cos \theta); \quad \lambda_c \equiv 2\pi / m \quad (32.2)$$

(remember that we're using units where $c \equiv 1$ and $\hbar \equiv 1$). The electron's *Compton wavelength* $\lambda_c = 0.02426 \text{ \AA}$.

In an outstanding series of experiments during 1921–1922 Compton determined the wavelengths of scattered photons from their diffraction by a crystal.⁷ His remarkable 1923 paper reported a measured value for λ_c of 0.022 \AA .⁸ Compton's results provided extremely strong evidence for the actual existence of Einstein's quanta of electromagnetic radiation. Referring to the conflict between said quanta (photons) and a theory of radiation based on Maxwell's equations, Einstein in 1924 remarked: "We now have two theories of light, both indispensable, but, it must be admitted, without any logical connection between them, despite twenty years of colossal effort by theoretical physicists."⁹ Resolution of this conundrum awaited the development of *quantum electrodynamics*.

⁷ Roger H. Stuewer, "Einstein's Revolutionary Light-Quantum Hypothesis," *HQ-1 Conference on the History of Quantum Physics*, Max Planck Institute for the History of Science, (2007): http://quantum-history.mpiwg-berlin.mpg.de/eLibrary/hq1_talks/keynote/34_stuewer/stuewer_hq-1_pres.

⁸ Arthur H. Compton, "A quantum theory of the scattering of x-rays by light elements," *Physical Review* **21**, 483 (1923): <https://journals.aps.org/pr/abstract/10.1103/PhysRev.21.483>.

⁹ David C. Cassidy, "Focus: Landmarks: Photons are Real," *Physical Review Focus* **13**, 8 (2004): <https://physics.aps.org/story/v13/st8>.

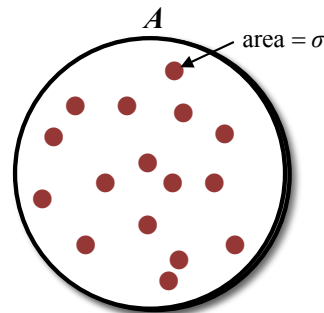
Dynamics: the Klein-Nishina formula (Experiment 32b)

Scattering cross section

Given the kinematics described by the Compton formula (32.1), what remains is to determine the probability of the scattering event depicted in Figure 2. This can only be calculated by considering the nature of the interaction between the photon and the electron. Thinking classically, of course, we would consider the “stream of photons” to be equivalent to an incoming beam of electromagnetic radiation. This radiation would exert Lorentz forces on any electrons present, causing them to oscillate. Each oscillating electron would in turn generate an outgoing pattern of electromagnetic radiation, which could then be interpreted as a somehow equivalent stream of scattered photons. The ratio of the intensities of the induced radiation to the incident radiation would then be interpreted as the probability of the scattering.

Scattering probability is normally expressed as a *scattering cross section*, which represents an “effective area” subtended by a stationary target as seen by a stream of incident particles. To see why this is so, consider Figure 3. In this simple scenario, the targets obstruct a fraction of the total cross sectional area of the incident beam as it passes through a volume containing them, each individual target obstructing an area σ . The fraction of the total incident beam area obstructed by the targets becomes the probability that any one incident particle is scattered. In this case, the area σ would represent the *total scattering cross section* of a single target.

Figure 3: A very thin section of a volume containing N target particles, each with cross sectional area σ . If the volume’s total cross sectional area is A , the targets obstruct a fraction $N\sigma/A$ of the area. On average, that fraction of a uniform beam of incident particles will encounter targets and be scattered.



This rough idea is made more rigorous by its development in this text’s *Appendix A*. You should read and thoroughly understand that material in order to follow the rest of this section. In that appendix you will also be introduced to the concept of $d\sigma/d\Omega(\theta, \varphi)$, the *differential cross section* for scattering toward a particular outgoing direction specified by the spherical coordinate angles (θ, φ) . Measuring the differential cross sections for scattering of the outgoing photon into various directions is the whole point of Experiment 32b.

Klein-Nishina scattering cross section

During the brief period 1926–1928 the young British theoretical physicist Paul Adrien Maurice Dirac wrote a series of papers which would revolutionize our understanding of the nature of the most fundamental laws of physics. His initially-controversial masterpiece, “The quantum theory of the electron,” not only incorporated the concept of electron spin (intrinsic angular momentum with no classical counterpart), but also predicted the existence of antimatter as an inseparable partner to matter (required by any consistent, relativistically-correct quantum theory).¹⁰

Dirac analyzed Compton scattering in 1926 while still a graduate student and derived the following differential cross section for the process (in this text’s *Appendix B* we derive this formula in a simple way very different from Dirac’s method):

$$\text{“Spinless” electron scattering: } \frac{d\sigma}{d\Omega} = \frac{r_e^2}{2} \left(\frac{k'}{k_0} \right)^2 (1 + \cos^2 \theta) \quad (32.3)$$

In this expression the ratio k'/k_0 is calculated at angle θ using the Compton scattering formula (32.1). The constant r_e is known as the *classical electron radius*, 2.818×10^{-15} m. It is discussed more thoroughly in the description of Thomson scattering in *Appendix B*. The final factor in (32.3) includes two terms: one for incident photons linearly polarized perpendicularly to the plane of scattering, the other for photons whose polarization lies in the scattering plane. The sum of these terms represents the overall rate of scattering for an unpolarized stream of incident photons.

Unfortunately, (32.3) neglects the fact that an electron has a magnetic moment generated by its intrinsic angular momentum (spin 1/2). This magnetic moment also interacts with the incident photons’ electromagnetic fields and serves as an additional scattering mechanism. Dirac’s 1928 papers provided the theoretical framework to properly calculate the additional effects of the electron’s spin, but that theory is more complicated, subtle, and difficult to apply. Oscar Klein and Yoshio Nishina worked feverishly in the months following Dirac’s publication to understand his ideas and apply them to Compton scattering, publishing their calculation only six months later.¹¹ By successfully including the effects of the electron’s spin, their result provided a slight

¹⁰ P. A. M. Dirac, “The quantum theory of the electron,” *Proc. Royal Soc. A*, **117**, 610 (1928): <http://rspa.royalsocietypublishing.org/content/117/778/610>; “...Part II,” *Proc. Royal Soc. A*, **118**, 351 (1928): <http://rspa.royalsocietypublishing.org/content/118/779/351>. Dirac’s papers during this period also introduced into quantum mechanics time-dependent perturbation theory, the mathematics of *commutators* and *spinors*, his *delta function*, and the *second quantization* of boson fields such as electromagnetism. The *positron* (anti-electron) was identified by the Caltech physicist Carl Anderson in 1932, and Dirac shared the 1933 Nobel Prize with Erwin Schrödinger. Anderson was awarded the 1936 Nobel Prize.

¹¹ O. Klein & Y. Nishina, “The Scattering of Light by Free Electrons according to Dirac’s New Relativistic Dynamics,” *Nature*, **122**, 398 (1928): <http://www.nature.com/articles/122398b0.pdf>. See also Footnote 24 in *Appendix B*.

modification (at first glance) to (32.3): the addition of another term to its final factor, shown in the following equation:

$$\frac{d\sigma}{d\Omega} = \frac{r_e^2}{2} \left(\frac{k'}{k_0} \right)^2 \left[1 + \cos^2 \theta + \frac{(k_0 - k')^2}{k_0 k'} \right]$$

This additional term due to photon scattering by the electron's magnetic dipole moment is also the result of an average over the possible orientations of the electron's spin (both before and after scattering) as well as the incident and scattered photons' polarizations. Clearly this term is positive, thus increasing the expected differential cross section at all scattering angles greater than 0. Its effect is evidently greatest for large incident photon energies and for large scattering angles. We may put this formula into its more common form by substituting $2 - \sin^2 \theta$ for $1 + \cos^2 \theta$, then expanding the numerator of the extra term and simplifying. The result is the famous formula:

Klein-Nishina scattering:
$$\boxed{\frac{d\sigma}{d\Omega} = \frac{r_e^2}{2} \left(\frac{k'}{k_0} \right)^2 \left(\frac{k'}{k_0} + \frac{k_0}{k'} - \sin^2 \theta \right)} \quad (32.4)$$

Other than an outline of the explanation of the anomalous Zeeman effect in atomic spectra given in Dirac's 1928 papers, this formula was the first formal result derived from his theory of the electron which was subject to available experimental tests of the time. It gives the expected rates for the scattering of high-energy photons into various angles θ . The ratio k'/k_0 and the constant r_e in (32.4) are defined the same way as in (32.3). Plots of (32.4) and (32.3) for the ^{137}Cs γ -ray used in Experiments 32 are shown in Figure 4.

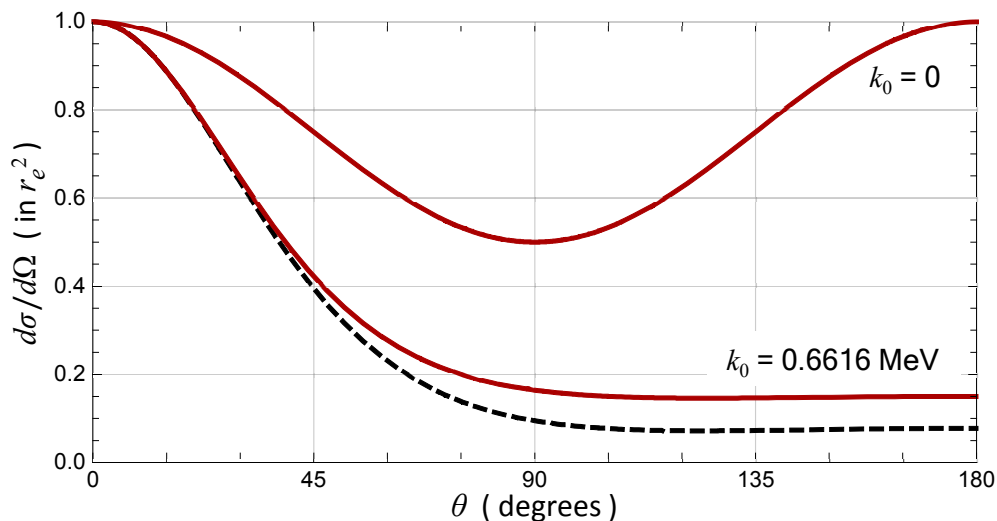


Figure 4: Klein-Nishina differential cross section for a Cesium-137 photon. Also shown is the cross section in the limit of very small photon energy, which is the same as the classical, Thomson cross section (see Appendix B). The dashed line shows the cross section given in equation (32.3), which neglects the electron's spin.

THE APPARATUS

Overview: capturing Compton events

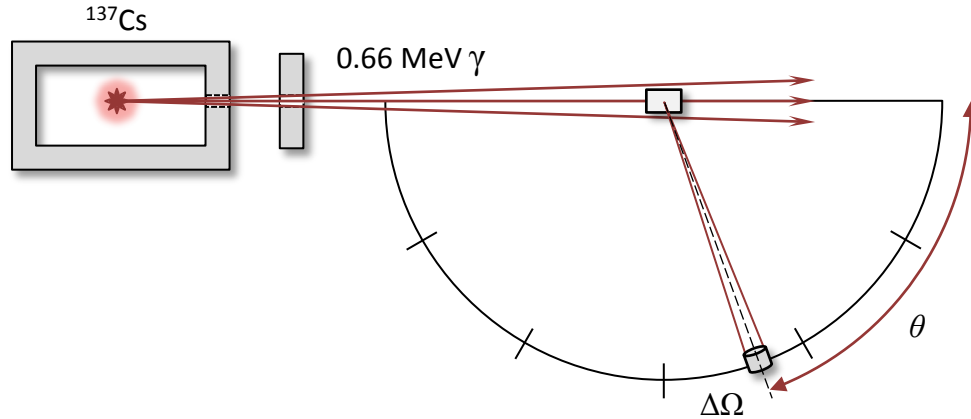


Figure 5: Setup for capturing and measuring Compton scattering events. Collimated γ -rays from a ^{137}Cs source illuminate a plastic scintillator (the target). A NaI scintillator is positioned at an adjustable angle θ away from the incident beam, intercepting a small solid angle $\Delta\Omega$. A scattering event is recognized by near-simultaneous detections in the target scintillator (outgoing electron) and the NaI scintillator (outgoing photon). The two scintillator outputs measure the kinetic energies of the outgoing particles. The center of the target volume is approximately 90cm from the ^{137}Cs source. The “protractor” radius for the NaI scintillator is approximately 40cm.

The setup for experiments 32a and 32b is diagrammed in Figure 5. Originally designed and constructed in 1975 by Caltech undergraduate Kevin Ruddell (BS '75), the basic concept is to use the apparatus to select for Compton events with a specific photon scattering angle θ . By using scintillators whose output pulse strengths can be measured using multichannel analyzers (MCAs, as in Experiment 30a), both the outgoing electron and the outgoing photon kinetic energies can be measured. Measurements are triggered by near-simultaneous detections in the two scintillators so that they may be associated with a single Compton scattering event. Incident high-energy photons are generated by a Cesium-137 source, which outputs $0.6616\text{ MeV } \gamma$ -rays and 32 keV x-rays. The direction of the incident photon stream is collimated using holes in the lead shielding surrounding the source.

The target of the incident photon beam is a small, rectangular piece of plastic scintillator material attached to a photomultiplier tube (PMT). The low atomic numbers of the scintillator atoms (predominantly carbon and hydrogen) ensure that Compton scattering is the dominant interaction of the incident photons with the target material. Its small size (see Figure 6 on page 9) ensures that it is uniformly illuminated by the incident photon stream. Its low density gives it an incident photon attenuation length (mean free path) of just over 9.6 cm (see Appendices A and C). Coupled with its depth of 3.5 cm , about 30% of the incident photons should be scattered by the target.

The outgoing photon scintillator is a sodium iodide (NaI) crystal as in Experiment 30a. Its diameter and distance from the target determine the solid angle $\Delta\Omega$ around the nominal scattering angle θ for which scattered photons are intercepted and can be detected. The scintillator's density and thickness ensures that it has a high probability of detecting any scattered photons which may enter it.

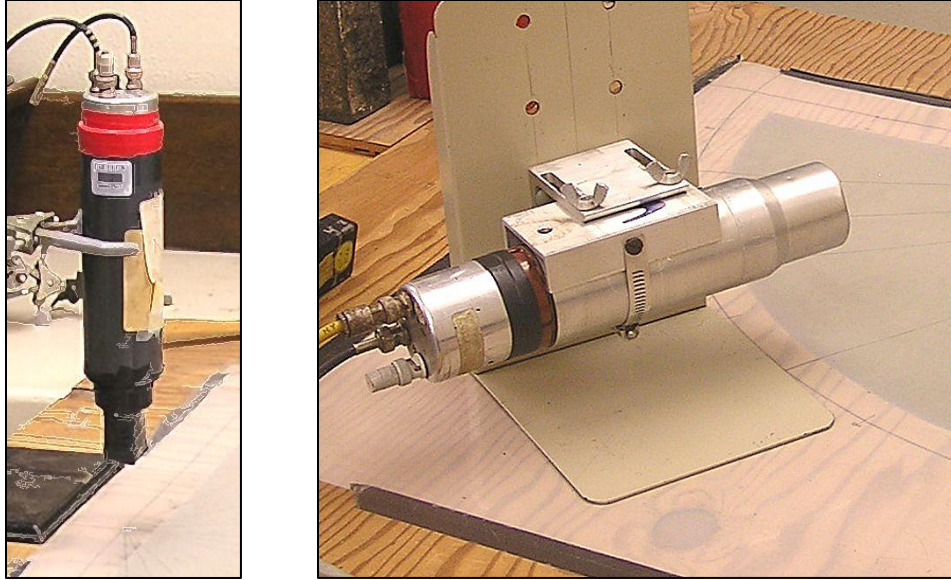


Figure 6: The target scintillator/photomultiplier (left) and the outgoing photon scintillator/photomultiplier (right). Viewed from the incident photon source, the plastic target scintillator is 1.9cm wide \times 3.6cm high \times 3.5cm deep. The 5cm diameter NaI photon scintillator may be positioned at various angles from the target using a large protractor (partially shown in the photo).

The selected scattering angle θ may be changed by varying the position of the outgoing photon scintillator (Figure 6). The experimenter can then collect data regarding both the outgoing particle energies and the scattering rate as a function of scattering angle. For Experiment 32a, the outgoing energies are the primary focus so that the kinematic Compton scattering formula (32.1) may be tested. Experiment 32b looks at the scattering rates in order to test the Klein-Nishina formula (32.4).

The relative positioning of the table protractor and the scintillators limit the accuracy with which the scattering angle θ may be determined. The uncertainty in θ is probably approximately $\pm 1^\circ$ (systematic) with an additional $\pm 1^\circ$ (random, independent).

The overall dimensions of the source and scintillator arrangement result in total photon path lengths of over a meter from source to outgoing photon scintillator. In addition, the scattering probability into the resulting $\Delta\Omega$ is expected to be quite small, especially for large θ (refer back to Figure 4 on page 7). Consequently, the incident photon source must be fairly strong in order to generate scattering data in a reasonable time. The ^{137}Cs source activity in 2018 is approximately

19 *milliCurie* (mC: 3.7×10^7 decays/sec), quite large compared to the ~ 1 *microCurie* (uC) sources used in Experiment 30a and for detector energy calibration in these experiments — thus the need for a heavy, lead-lined box to contain the source.

The scintillator photomultiplier tubes (PMTs) are designed to output current pulses with integrated charges proportional to the energies deposited in the scintillators. The next section describes the PMT pulse processing electronics used in the experiments.

Pulse processing electronics

The target and outgoing photon scintillators generate light which is detected by their attached photomultiplier tubes (PMTs). Following a single photon detection event, the output of a PMT is a tiny current pulse whose total integrated charge is designed to be proportional to the energy of the light pulse produced by its scintillator. In the target scintillator this corresponds to the kinetic energy of the outgoing electron following a Compton scattering event. In the outgoing photon scintillator it corresponds to the interaction of the scattered photon with an atom in its sodium iodide (NaI) crystal. The current pulses generated by the scintillator PMTs are processed by the experiment's electronics system to identify Compton scattering events and to measure and record the integrated charges of the two PMT pulses associated with these events. Figure 7 provides a cartoon illustration of the experiments' electronics, identifying its major components.

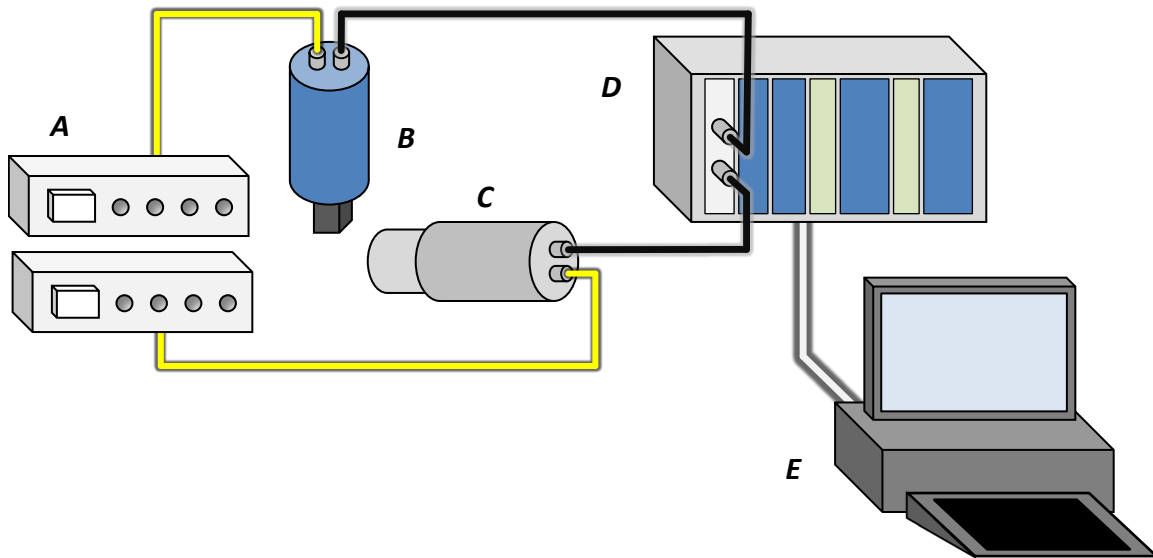


Figure 7: Electronics used to process and record Compton scattering events. A: high voltage power supplies for the scintillators' photomultipliers; B: target scintillator/photomultiplier; C: outgoing photon scintillator/photomultiplier; D: signal processing electronics (coincidence detection and pulse energy measurement); E: computer control and data capture.

High voltage power supplies (HVs) activate the scintillators' PMTs. The incoming photon rate from the ^{137}Cs source is quite high, so the average output current produced by the many target

PMT pulses is relatively large. Consequently, its power supply must be able to source relatively high currents to the PMT in order to mitigate inaccuracies caused by rate-related gain shifts. The pulse processing electronics system does not have gain adjustments accessible to the experimenter, so the HV supply voltages to the PMTs must be adjusted to set the system gains.

The pulses from each PMT are processed in parallel by essentially identical electronics, as diagrammed in Figure 8.

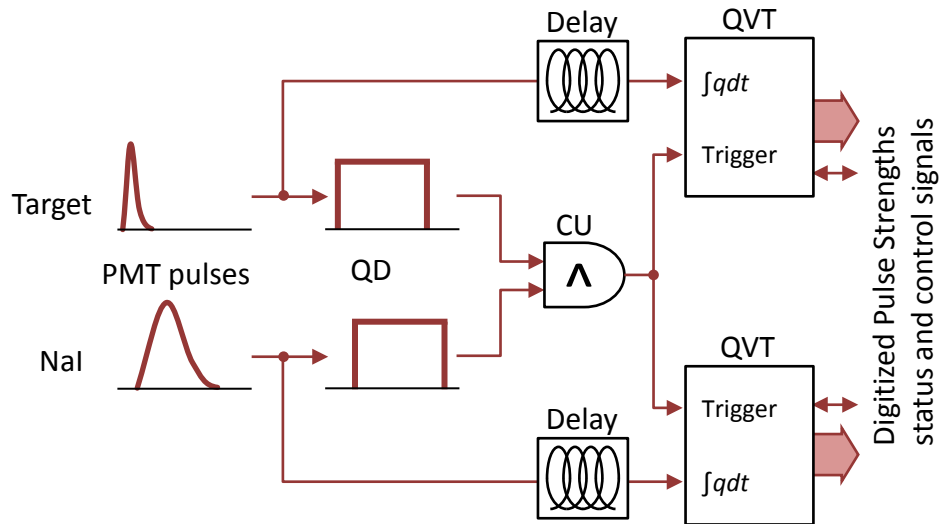


Figure 8: Signal flow from the scintillator photomultipliers (PMTs) to the digitizers (QVTs). First the PMT output pulses are aligned in time by using lengths of coaxial cables to match the pulse delays. As they are routed to their respective charge-integrating analog-digital converters (QVTs), the PMT pulses also generate digital event signals using two sections of the Quad Discriminator unit (QD). If the event signals overlap, the Coincidence Unit (CU), which is just a fancy logical AND gate (“ \wedge ”), generates a trigger event, which in turn enables the QVTs to digitize only these coincident PMT pulses. Delays are inserted into the pulse signals using coiled lengths of additional cable to ensure that the trigger signals arrive at the QVTs just before the PMT pulses.

The signal processing scheme proceeds as follows (refer to Figure 8 as you follow along):

1. Match the two scintillator/PMT pulse output delays by using an appropriate length of signal cable between each PMT output and its electronics input (5 ns/meter propagation delay in a signal coaxial cable).
2. Divide each PMT pulse output into two parallel signal chains: analog pulse integration for multichannel analyzer (MCA) measurement, and digital event coincidence detection for MCA triggering.
3. Event coincidence detection starts by first amplifying each PMT pulse output and then comparing it to a threshold level with a *discriminator* (a single channel of a Quad Discriminator unit, QD). If a PMT pulse exceeds its threshold, the QD outputs a digital event pulse. The threshold level is set high enough to reduce false event detections caused by noise.

4. The event pulses from the two PMT channels are input to a *coincidence unit* (CU). This device continually performs a logical *AND* of its inputs. Whenever PMT event pulses at the CU inputs overlap in time, the CU's *AND* function is satisfied, and it outputs a digital *coincidence pulse*.
5. The CU coincidence pulse is connected to the Trigger inputs of the two pulse MCA digitizers (called QVTs for their charge-voltage-time measurement modes). The presence of a trigger pulse enables each QVT to respond to the next analog PMT pulse arriving at its signal input.
6. While the digital coincidence processing goes on, the analog PMT pulses continue along additional coaxial cabling to QVT *charge integrating* (Q) signal inputs. The cables slightly delay these pulses so that a CU coincidence pulse arrives at the QVT Trigger inputs first.

A custom *interface unit* (IU, not shown in Figure 8) for each QVT controls its operation and provides a computer control interface. When a QVT unit digitizes its PMT pulse following a trigger event, it signals the IU and provides the digitized PMT pulse strength value. The IU immediately disables the QVT (so that it won't respond to additional pulses) and signals the control computer that it has QVT data available. When the computer sees that both QVTs have digitized data for their respective PMT pulses, it reads the data and then signals the IUs to enable their QVTs to respond to another event. Computer software (described in the next section) performs the MCA function to generate scintillator energy spectra from the QVT data.

Software

Two application programs will be used to control the experiments' data acquisition and generate scintillator energy spectra: *MCA*, used to generate scintillator spectra from each individual QVT in order to set system gains and perform energy calibrations; and *Compton Experiment*, used to collect coincidence data from both QVT channels in order to correlate target and outgoing photon scintillator energies and event rates with scattering angle. The operation of each application is described in the following sections. For data analysis, the *Exp32.nb* notebook augments *CurveFit* with functions useful for displaying and analyzing coincidence MCA data.

MCA application

The *MCA* application software is used for individual scintillator energy calibration. It controls a single QVT unit and creates a standard MCA histogram of event counts vs. channel number. The user can select which QVT unit to control (target or outgoing photon), so MCA histograms can be obtained from each of the two detectors for the several calibration γ -ray sources. MCA histograms are saved as *CurveFit *.mca* data files, which can then be input as ***Standard CurveFit Data Files***. The data are in the format *x*: MCA channel, *y*: event counts. An example of the MCA application user interface window is shown in Figure 9.

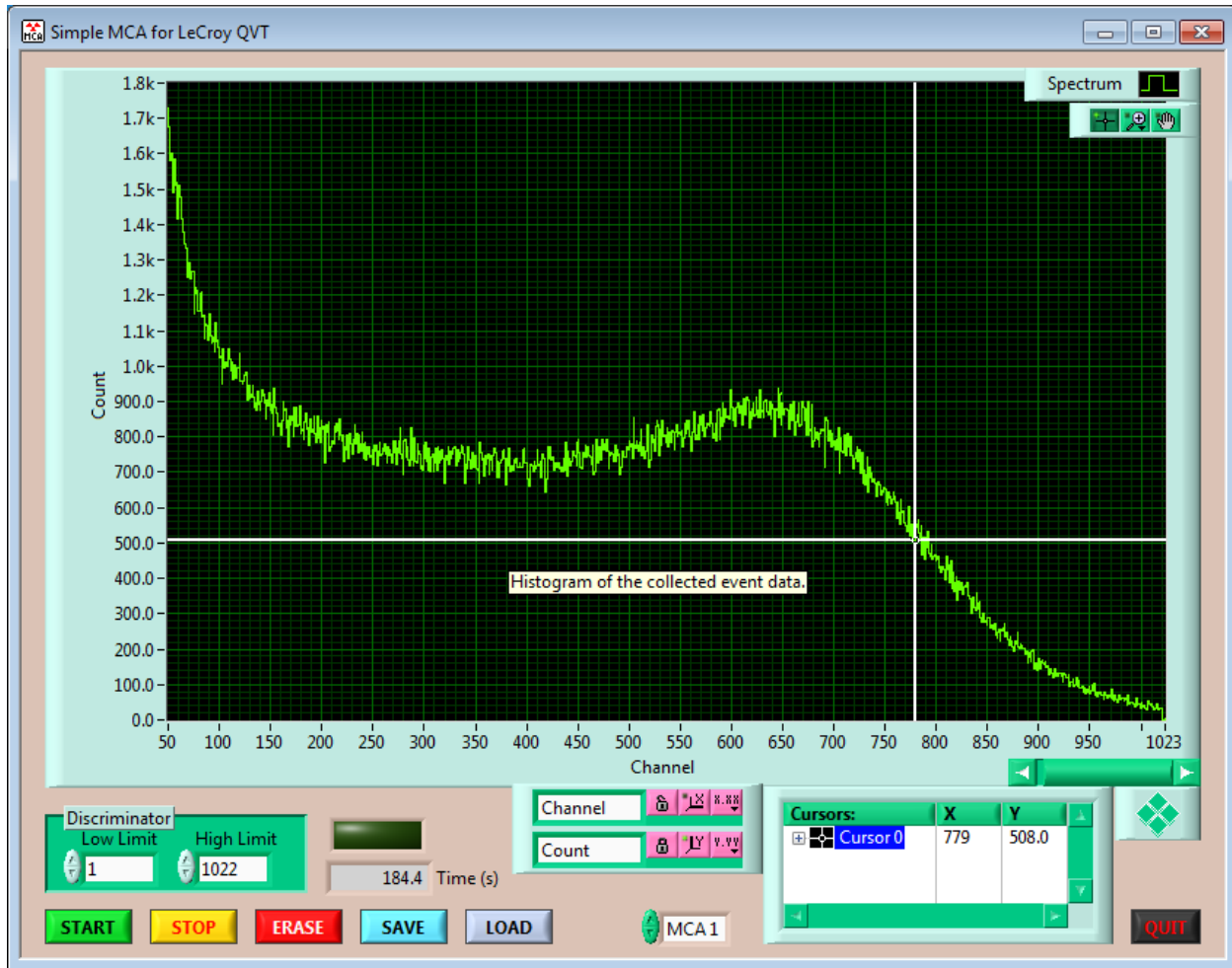


Figure 9: Sample MCA application user interface window. The displayed histogram is of a Cs137 calibration source using the plastic (target) scintillator. The low atomic number of the carbon atoms in this scintillator makes photoelectric absorption of the 0.6616 MeV gamma photons very unlikely, so only a Compton spectrum is evident. The MCA application controls are very basic. The MCA selector chooses the scintillator to use: “MCA 1” selects the target scintillator, “MCA 2” the NaI scintillator.

Compton Experiment application

The *Compton Experiment* application software is used to collect coincidence data from both QVT units. It controls both the target and outgoing photon QVTs, and collects event data consisting of pairs of MCA channel numbers, one value from each QVT. It creates MCA histograms for both detectors from the coincidence event data. Additionally, it can create a scatter data plot of all of the individual event channel pairs. When data are saved, it creates *.x.mca and *.y.mca histogram files for the target and outgoing photon detectors, respectively. Each of these is a *Standard CurveFit Data File* with the format x : MCA channel, y : event counts. It also creates a large *.xy.mca data file which contains coincidence channel pairs for every detected event with the format x : target MCA channel, y : outgoing photon MCA channel. The main user interface window is shown in Figure 10; the scatter plot window in Figure 11.

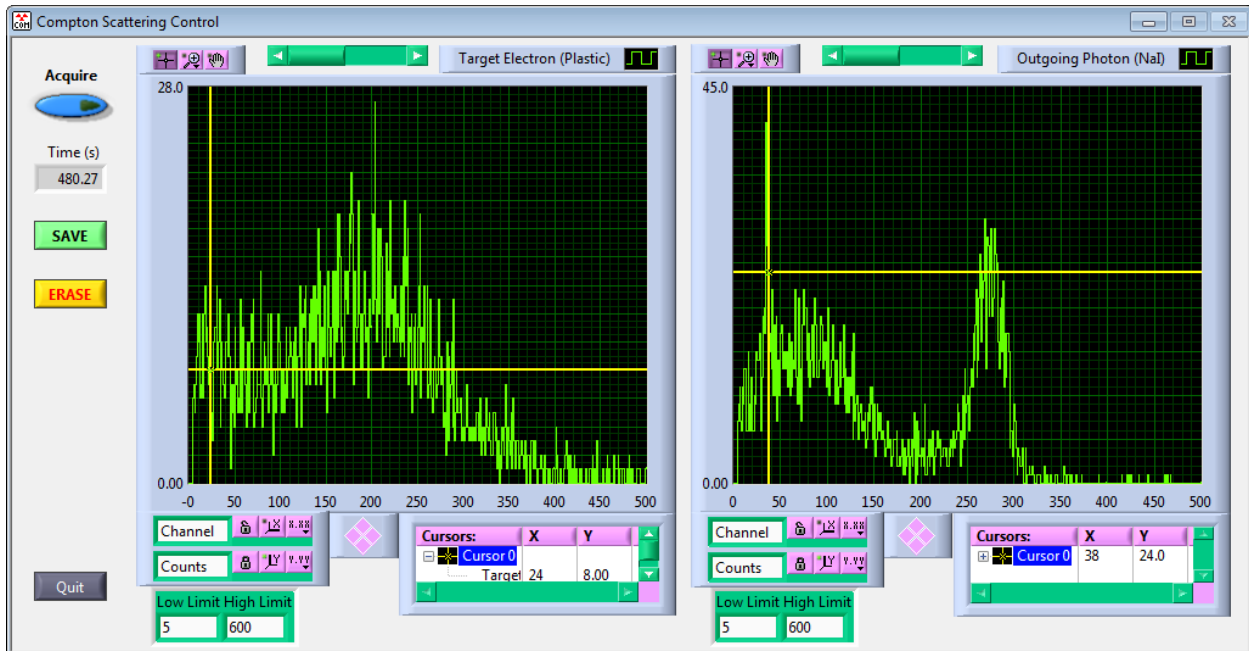
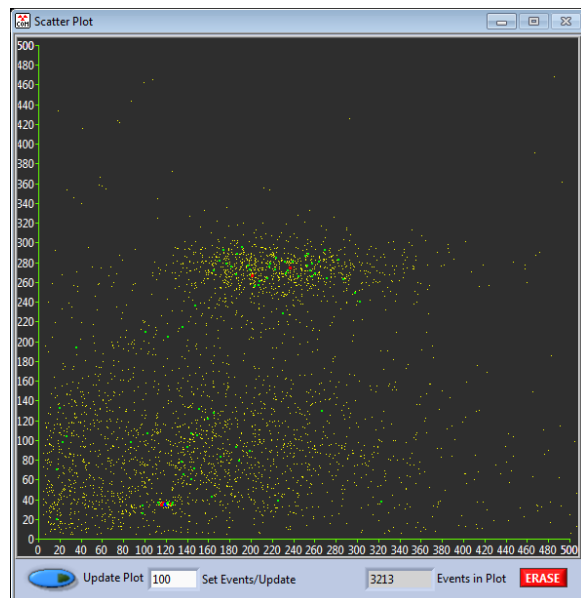


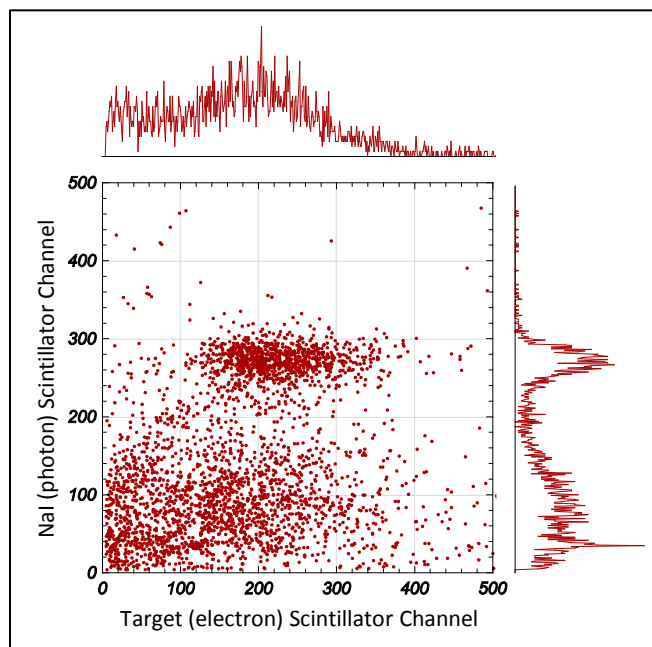
Figure 10: *Compton Experiment* application main window. MCA histograms of both the target and NaI scintillators are generated from the coincidence event detections. As with the MCA application, the user interface is quite simple. The MCA histograms shown were generated with the NaI scintillator set at angle θ equal to 60 degrees.

Figure 11: The *Compton Experiment* scatter plot window. Activating and erasing this plot and its data is controlled independently of the data in the main window. If there are many thousands of points in the plot, then it may cause a noticeable time delay when updated. The user can select how many points to collect between plot updates so that the time impact is mitigated. The scatter plot shown was generated from the set of events also displayed in Figure 10.



Interpreting scatter plots

Figure 12: The relationship between the event scatter plot (from Figure 11) and the individual scintillator channel histogram data plots (from Figure 10). The scintillator histograms provide projections of the events onto their respective axes, x for the target scintillator and y for the outgoing photon (NaI) scintillator. Each histogram channel then provides a count of the number of events projected into that particular channel.



Careful interpretation of an event scatter plot and its corresponding scintillator histograms is key to proper analysis of your experimental results (see Figure 12). Even when the angle θ to the outgoing photon (NaI) scintillator is held fixed, the scatter plot is complicated by the many possible combinations of photon interactions in the two scintillators which may result in a particular event detection. Possibilities include various combinations of one or more Compton scatters in the target scintillator followed by Compton scatters and/or photoelectric absorption in the outgoing photon (NaI) scintillator (we disregard the very rare possibility of photoelectric absorption in the target scintillator). In addition, a scattered photon leaving the target may Compton scatter off of the table supporting the apparatus or some other object and then enter the NaI scintillator, triggering an event detection. Lastly, two incident photons may scatter in the target nearly simultaneously, the outgoing photon of one of which may then enter the NaI scintillator.

Disregarding the final two possibilities detailed above, a single incident photon deposits some fraction of its energy into the target scintillator through Compton scattering. The scattered photon then enters the NaI scintillator, depositing some or all of its energy depending on whether it is photoelectrically absorbed or only Compton scatters. The energies deposited in the two scintillators determine the respective channel numbers of the event. If the scattered photon is photoelectrically absorbed, then all of the original, incident photon's energy (0.6616 MeV from the ^{137}Cs source) is split between the two scintillators. The oval cluster near the center of the scatter plot in Figure 12 contains events which correspond to a single Compton scatter in the

target followed by photoelectric absorption in the NaI detector. Note the “full energy” peak in the NaI (y -axis) histogram aligned with this cluster of events.

The various other possibilities described above result in events falling into other regions of the scatter plots. Consider the left-hand graphic shown in Figure 13, which contains the same data as Figure 12. Regions 1 and 2 of the plot contain events which involve a single Compton scatter in the target followed by either photoelectric absorption or Compton scattering of the outgoing photon in the NaI scintillator. These are the events we are most interested in. Region 3, filling most of the rest of the plot, includes events which involve multiple Compton scatters in the target whose final outgoing photons happen to be detected by the NaI scintillator.

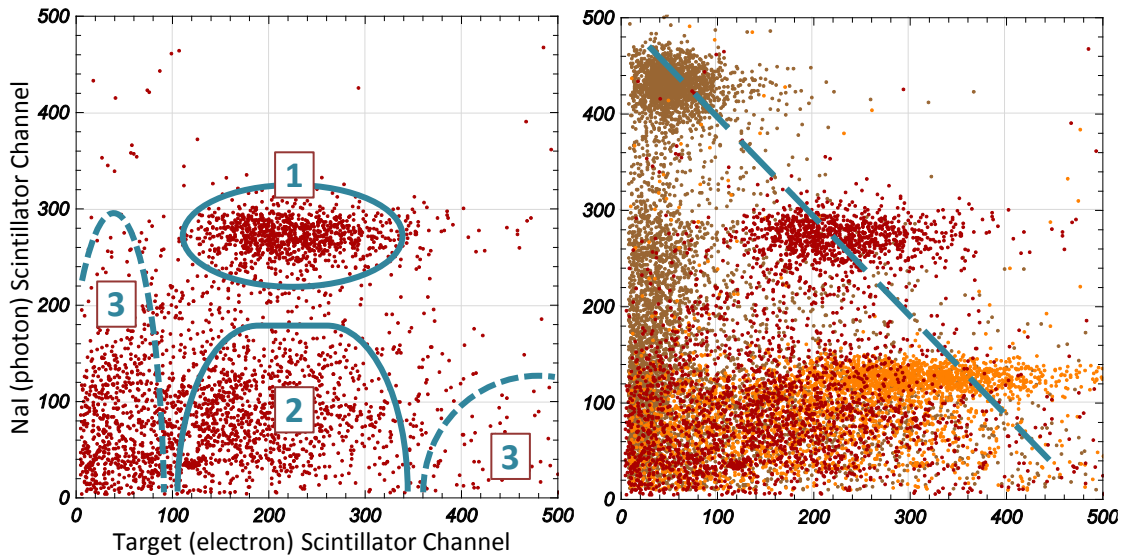


Figure 13: Scatter plots illustrating the various regions into which events may fall. The left-hand plot is for an outgoing photon scintillator angle of 60° . The significance of the variously identified regions of the plot is explained in the text. The right-hand plot is a superposition of three event data sets: 20° (brown), 60° (red), and 150° (orange). The diagonal blue line shows the trend in the position of the oval cluster of events (corresponding to region 1 in the left-hand plot) as the angle to the NaI scintillator is changed.

The right-hand graphic of Figure 15 shows how the scatter plot changes with the deflection angle θ to the NaI scintillator (results for angles of 20, 60, and 150 degrees are shown). The diagonal blue line shown in the plot roughly represents the locus of points for which the sum of the energies deposited in the two scintillators is equal to the incident photon energy, k_0 . Events below this line could be due to a single photon causing detections in the two scintillators, whereas events above this line would require a coincidence of two incident photons scattering in the target nearly simultaneously. The few points in the upper right-hand region of the plot indicate how infrequently this combination occurs. Because the scintillation detectors have relatively poor energy resolution (especially the plastic target scintillator), the line dividing these two regions is fuzzy. The three oval-shaped event regions corresponding to region 1 of the left-hand figure nicely illustrate this fact.

EXPERIMENT 32a

Purpose of the experiment

The purpose of this experiment is to evaluate the accuracy of the kinematic Compton scattering formula, equation (32.1). If this equation accurately describes the variation of outgoing photon energy versus scattering angle, then Einstein's theory that electromagnetic radiation can behave as though it were composed of discrete, massless particles (quanta, photons) with energies $E = \hbar\omega$ has received very strong support. Your data will provide evidence to help decide this question.

Procedure

Once you have familiarized yourself with the setup and electronics, the procedure divides into two distinct phases, each described in detail below.

Detector calibrations

Do not start the MCA application if the Compton Experiment application is running. Quit the Compton Experiment application first.

Using the *MCA* application, you will adjust the individual detector high voltages (target and NaI) and collect gamma ray calibration spectra using the same sources and the same procedure you used for Experiment 30a, among others. Keep the main ^{137}Cs source blocked with lead brick during the calibration data collection; use only the various gamma ray sources you have used previously in other experiments.

Apply the high voltages to the two detectors by activating their power supplies.

To select a particular detector for collecting calibration spectra, you must select the correct MCA (MCA1 or MCA2) using the control on the *MCA* application display, and you must also select the button corresponding to that detector on the *Coincidence Unit* (CU). The other detector's button should be deselected.

Using a ^{137}Cs calibration source, adjust the detector HV power supply voltages so that the 0.661 MeV photon full energy peak fits just below channel 500 in the NaI scintillator MCA spectrum, and its Compton edge fits just below channel 500 in the target scintillator MCA spectrum. With these voltage settings, the scatter plots you collect later will contain all of the relevant events.

Once the detector power supply voltages are properly set, collect and save MCA spectra of the various gamma ray sources for later analysis and calibrations of the target and NaI MCA channel energies. Make a note of what range of low channel numbers in each detector's spectra seem to consistently contain a significant amount of noise event counts.

Record in your lab notebook the known photon energies and your observed channel numbers for the various full energy peaks found in each NaI detector calibration spectrum.

Not many of the calibration sources will provide clean enough Compton edge features to be useful for calibrating the target detector. Your NaI detector calibration should be quite good, however.

Compton scattering energy vs. angle data collection

Once you have collected and saved the calibration spectra for both detectors, **quit the MCA application**. Start the *Compton Experiment* application.

Do not start the *Compton Experiment* application until after you have quit the MCA application.

Push in both buttons on the *Coincidence Unit* (CU), one button for each of the two detectors. Now only coincidence events will be recorded.

Examine the alignment of the target scintillator with the protractor used to measure NaI detector scattering angle. If necessary, consult your TA and adjust the target scintillator position.

Remove the lead brick blocking the main ^{137}Cs source. Return any calibration sources to their storage area.

Set the NaI detector along the circumference of the protractor at an angle of about 40° and carefully record the angle and the distance between the center of the NaI scintillator and the center of the protractor.

Compton Experiment application setup: On the *Scatter Plot* window, activate the *Update Plot* control, enter '50' in the *Set Events/Update* control, and *Erase* the display. On the *Compton Scattering Control* window, adjust the *Low Limit* channel number for each of the MCA displays to just above any significant noise channels you observed during calibration. *Erase* any displayed spectra and activate *Acquire*.

After two or three minutes you should see a well-defined full-energy peak in the NaI scintillator spectrum. The lower half of the target scintillator spectrum should display a broad peak. These features roughly correspond to an oval-shaped locus of events in the scatter plot, corresponding to region 1 in the example spectrum shown in the left-hand graphic of Figure 13 on page 16. Stop the acquisition and deselect the *Update Plot* control on the *Scatter Plot* window.

If the spectra appear as described above, save the event data. Three files will be created: one for each of the scintillator spectra and one for the event scatter plot. This is your first data point for the experiment.

If the spectra do not appear as described, then consult with you TA and the lab instructor to troubleshoot the problem.

If all seems to be working, reposition the NaI scintillator to a different angle and acquire more data. The procedure steps for collecting all events into the scatter plot are as follows:

- (1) Activate the *Update Plot* control on the *Scatter Plot* window;
- (2) select *Erase* on both windows to clear all data;
- (3) select *Acquire* and collect the event data.
- (4) deselect *Acquire* and then deselect *Update Plot* when the data are sufficient;
- (5) save the data. **Record the channel numbers of the scintillator peaks along with the NaI detector position angle in a table in your lab notebook.**

You need to cover a wide range of angles in order to test the kinematic Compton scattering formula.

Securing the experiment

Set the HV power supplies for the two detectors to *Standby*. Block the beam from the ^{137}Cs source. Return any calibration gamma-ray sources to their proper storage containers. Quit the *Compton Experiment* application.

Analysis

You should include tables of the channel numbers (with uncertainties) both for the scattering data (function of θ) and calibration data (function of calibration source photon or Compton edge energy).

Your analysis should include plots of a few representative energy spectra of the plastic (target) and NaI scintillators, both of calibration spectra and of Compton scattering spectra. You should also include a few representative scatter plots of the Compton scattering data showing plastic channel number (x -axis) vs. NaI channel number (y -axis). See the subsection below concerning scatter plots in *CurveFit* and *Mathematica*®.

For a representative scatter plot, you should describe the features of the data point densities in the plot with an explanation of the processes or scattering geometries which may have generated them.

Rearranging equation (32.1) gives an equation similar to (32.2):

$$\frac{1}{k'(\theta)} = \frac{1}{k_0} + \frac{2}{m_e} \sin^2 \frac{1}{2}\theta \quad (32.5)$$

This equation is a linear relationship between functions of your two experimental quantities θ and k' . The slope of the relation is related to the electron's rest energy m_e , and the intercept to the γ -ray energy k_0 .

To test the relationship in (32.5), you must first calibrate the NaI scintillator energy scale (channel number vs. energy) using the full-energy peaks in your calibration spectra. This calibration may then be used to convert your scattered photon full-energy peaks to energies $k'(\theta)$. These experimentally-determined energies will have both systematic (from your calibration) and independent random uncertainties. As mentioned in the description of the apparatus, your recorded scattering angles θ will also have both systematic and independent, random sources of error and their associated uncertainties. Make sure you correctly consider how each of these sources of uncertainty will propagate into your analysis.

Although your calibration spectra for the target scintillator are insufficient to generate a precise energy calibration, you can perform a rough calibration of that scintillator. Compare your target scintillator energy peak vs. angle data to what you would expect for the outgoing electron kinetic energy following a Compton scatter. Are your data consistent with energy conservation by the scattering interaction?

Data analysis Mathematica® notebook

The Mathematica® notebook *Exp32.nb* has a few useful functions for manipulating event scatter plot data (the *.xy.mca data files saved by the *Compton Experiment* application). As of this writing, the *CurveFit* functions it defines include:

- KeepXY[]: Uses an interactive dialog box similar to the *Keep an X range* selection in *CurveFit*. Using it you can select a rectangular region of a scatter plot to keep as a new data set.
- RemoveXY[]: Use its interactive dialog box to select a rectangular region of a scatter plot to remove from the data set.
- xy2y[]: Creates a *Y* (NaI scintillator) spectrum of the scatter plot events and assigns Poisson count uncertainties.
- xy2x[]: Creates an *X* (Target scintillator) spectrum of the scatter plot events and assigns Poisson count uncertainties.

For example, consider the sample scatter plot in the left-hand graphic of Figure 13 on page 16. you could use KeepXY[] to select only a small rectangular area surrounding the oval-shaped *region 1* of the scatter plot. Then using xy2y[] would give a spectrum containing mostly the NaI scintillator full-energy events. Fitting a Gaussian+constant function to this data would provide a good estimate of the outgoing photon's energy. Similarly, fitting the results from using xy2x[] on the scatter plot data subset could provide a good estimate of the target electron's kinetic energy.

Download the notebook

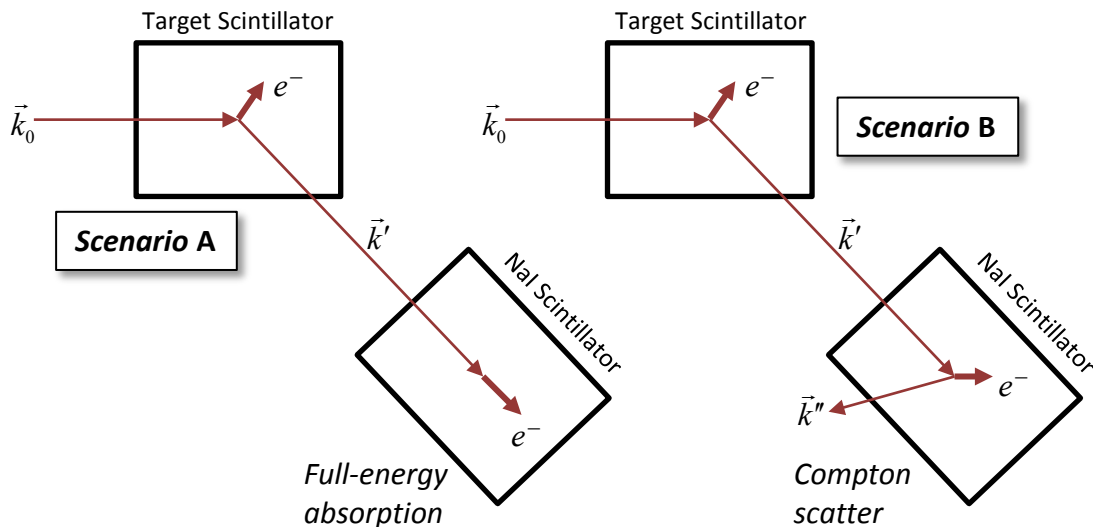
at: http://www.sophphx.caltech.edu/Physics_7/Mathematica_Notebooks/Exp_32/

Optional investigation

A possible additional investigation is to use your data to put a bound on the gamma-ray rest energy (it should, of course, be zero if photons are massless). Assuming that the photon rest energy is very small compared to that of the electron, can you derive a modification to (32.5) which includes the lowest order correction for a nonzero photon/electron rest energy ratio? You could then use your data to put an upper bound on this ratio.

Prelab Problems

1. Derive equation (32.2) from (32.1). With the electron's rest energy of 0.511 MeV and $\hbar c = 1970 \text{ eV}\text{\AA}$, show that $\lambda_c \approx 0.024 \text{ \AA}$. What is the wavelength (in \AA) of a 0.6616 MeV photon?
2. For an incident photon energy of 0.6616 MeV, use the kinematic Compton scattering formula to generate a plot of the expected outgoing photon energy (in MeV) as a function of scattering angle θ for $\theta = 0^\circ$ to $\theta = 180^\circ$.
3. The *Compton edge energy* is defined as the outgoing kinetic energy of an electron following a Compton scattering event for which the outgoing photon $\theta = 180^\circ$. What is the Compton edge energy for a 0.6616 MeV ^{137}Cs γ -ray? What about for a 0.511 MeV electron-positron annihilation photon from ^{22}Na ? At what outgoing photon angle θ must a 0.6616 MeV γ -ray be scattered for the electron's kinetic energy to equal the 0.511 MeV photon's Compton edge energy? What is the outgoing photon's energy in this case?
4. Show that if an incoming photon is Compton scattered by 90° and then the outgoing photon is scattered again by another 90° , then the final outgoing photon has the same energy as that from a single 180° scatter of the original incoming photon. Starting with equation (32.5) on page 19 is a particularly convenient way to perform this analysis.
5. Consider the following two scenarios for a possible Compton event detection:



Which region of the scatter plot shown in the left-hand graphic of Figure 13 on page 16, region 1, 2, or 3, contains events described by scenario A above? scenario B?

EXPERIMENT 32b

Purpose of the experiment

In Experiment 32a you evaluate the *kinematic* Compton scattering relationship, equation (32.1) or (32.5). This experiment supplements that result by investigating the *dynamics* of the photon-electron interaction. This dynamical relationship was derived from Dirac's theory by Klein and Nishina, resulting in equation (32.4) for the scattering cross section. Your goal is test this expression by measuring the Compton scattering rates into various outgoing photon angles. Complicating your analysis is the requirement to apply various corrections to your raw rate data to account for experimental effects such as detector efficiency and target self-absorption.

Procedure

Read completely through each section of the procedure before starting it. Make sure that you have a good plan for your data collection, and that you have the measurements you need to complete the analysis.

Electronics setup

Do not start the MCA application if the Compton Experiment application is running. Quit the Compton Experiment application first.

Start this experiment the same way as Experiment 32a: Leaving the main ^{137}Cs source blocked, activate the detector power supplies and use the MCA application to collect spectra from each detector. Using a ^{137}Cs calibration source, adjust the HV power supply voltages to limit the observed ^{137}Cs spectrum to the first 500 channels in each detector. Remember to select the appropriate MCA number in the MCA application and to only select the appropriate button on the Coincidence Unit (CU) for the detector to be used.

There is no need to perform detailed energy calibrations of each detector for this experiment, as you are interested in measuring scattering rates. Accurate energy measurements were required in Experiment 32a, but not in Experiment 32b.

Geometry measurements

In order to calculate absolute area numbers for the differential scattering cross sections, you must know the solid angle $\Delta\Omega$ into which detected photons are scattered. To determine this angle you must know the dimensions of the target and NaI scintillators and the distance between them. You must also know the distance between the ^{137}Cs source and the target scintillator, along with the scintillator dimensions, so that you can use the source decay rate to determine the rate at which gamma ray photons enter the target scintillator.

Do not start the *Compton Experiment* application until after you have quit the *MCA* application.

Compton scattering rate vs. angle data collection

Once the detector HV power supply voltages are properly set, quit the *MCA* application, select both detector buttons on the CU, and start the *Compton Experiment* application.

Accurate rate calculations require accurate acquisition time determinations, so don't set the *Set Events/Update* control on the *Scatter Plot* window to too low a value; 150 to 200 should be a good number (updating the scatter plot takes time if there are many events in the plot). To ensure that all relevant events are included in the plot, you must operate the *Compton Experiment* controls in the following order:

- (1) Activate the *Update Plot* control on the *Scatter Plot* window;
- (2) select *Erase* on both program windows to clear all data;
- (3) select *Acquire* and collect the event data.
- (4) deselect *Acquire* and then deselect *Update Plot* when the data are sufficient;
- (5) save the data.

Your strategy for selecting scattering angles for your measurements should be different from that used in Experiment 32a. Here you are interested in accurately determining the variation in event rate with scattering angle, so you need more data in the parameter space where the rate changes rapidly with changing angle. Look again at Figure 4 on page 7. The predicted scattering rate is very nearly constant for angles beyond about 100° , so few data points should be needed in that region. Conversely, angles from 20° to 90° show a rapid change in scattering rate, so your data in this region should be much more extensive. The lower the rate, the longer it will take to acquire accurate data, so you must also keep this fact in mind as you build up your data set.

As you change the angle to the NaI detector, carefully determine its position so that you can calculate the solid angle $\Delta\Omega$ into which detected photons are scattered at that nominal θ .

Securing the experiment

Set the HV power supplies for the two detectors to *Standby*. Block the beam from the ^{137}Cs source. Return any calibration gamma-ray sources to their proper storage containers. Quit the *Compton Experiment* application.

Analysis

Overview

You will need a thoughtful analysis to concentrate on the relevant events in your raw data and to then properly apply the several needed corrections to your measured scattering rates. Consider again the Klein-Nishina formula, equation (32.4), repeated below:

$$\frac{d\sigma}{d\Omega} = \frac{r_e^2}{2} \left(\frac{k'}{k_0} \right)^2 \left(\frac{k'}{k_0} + \frac{k_0}{k'} - \sin^2 \theta \right) \quad (32.4)$$

The purpose of the analysis is to use your experimental data to derive the differential cross section's dependence on the scattering angle θ and then compare your result to that predicted by the right-hand side of (32.4).

For some outgoing direction θ the differential cross section $d\sigma/d\Omega|_{\theta}$ indicates the differential probability of an incident photon scattering into that angle. Since both the incident photon rate at the target and the number of scattering sites (electrons) in the target are constants, the differential rate that photons scatter from the target into angle θ should be proportional to $d\sigma/d\Omega|_{\theta}$, at least at first glance. The observed rate at the NaI detector when placed at an angle θ , however, is influenced by a number of additional effects which require corrections to your raw data. These effects are discussed in the following sections.

Solid angle captured by the detected events

From the point of view of the photon-electron scattering site in the target scintillator, the cross-sectional area of the NaI scintillator detector subtends a small solid angle $\Delta\Omega_D$ about its placement angle θ . The solid angle subtended is given by its cross-sectional area divided by its separation from the target squared. Similarly, the target scintillator subtends its own small solid angle $\Delta\Omega_T$ about the angle θ (as seen from the position of the NaI scintillator), again given by its projected cross-sectional area divided by the scintillators' separation squared. To lowest order, the total solid angle captured by the event detection is given by the sum of these two:

$$\Delta\Omega = \Delta\Omega_D + \Delta\Omega_T = (A_D + A_T)/r^2 \quad (32.6)$$

where the areas A_D and A_T are the projected cross-sectional areas of the scintillators along the angle θ , and r is the distance between them. The scattered photon rate (ignoring other corrections, and to lowest order) will then vary as $\Delta\sigma = d\sigma/d\Omega|_{\theta} \Delta\Omega$. The face of the NaI scintillator has a diameter of 5.1 cm; the target scintillator dimensions are 1.9 cm wide \times 3.6 cm high \times 3.5 cm deep (as seen by the ^{137}Cs source).

The NaI scintillator should be oriented so that its circular face is normal to the line between its and the target scintillator's centers, so the area it subtends is always equal to the area of its

circular face. The target scintillator, however, because of its fixed position and rectangular, box-like volume, subtends an effective projected area which varies with scattering angle θ . It can be shown that its effective area is determined by the product of its height (3.6 cm) and the projected length of a diagonal of its base (choose the diagonal which gives the longer projected length normal to the direction θ). The common length of these diagonals is given by Pythagoras to be 4.0 cm; their angles from the target centerline are $\pm 28.5^\circ$. The projected target area A_T to be used in (32.6) is then given by:

$$A_T = (3.6 \text{ cm} \times 4.0 \text{ cm}) \times \max[\sin(\theta \pm 28.5^\circ)] \quad (32.7)$$

This equation means that you must pick the sign of the 28.5° which gives the larger result for A_T , + for $\theta < 90^\circ$, – for $\theta > 90^\circ$.

Example calculation: When the NaI scintillator is positioned at a scattering angle of 60° and at a distance of 40 cm from the center of the target scintillator, the projected areas subtended by the target and NaI scintillators are 14.3 cm^2 and 20.4 cm^2 , respectively, using (32.7) to calculate the target's projected area. The total solid angle calculated using (32.6) is then 0.022 steradian, about 0.17% of the unit sphere (4π steradian). Because the aspect of the target scintillator as seen by the NaI detector changes with θ , so will the solid angle it subtends. The observed detection rate must be divided by the total solid angle $\Delta\Omega$ to correct for this variation.

Correct the observed event rate at each θ by *dividing* by the total solid angle calculated using (32.6) and (32.7).

NaI detector efficiency corrections

Not all photons which enter the NaI scintillator will be detected. The scintillator's mass attenuation coefficient (*APPENDIX C: Mass attenuation coefficients*) provides a measure of the NaI detector's probability of detecting an incoming photon. The probability that a photon entering the scintillator has an interaction and is detected is given by:

$$P_{NaI} = 1 - e^{-\rho(\mu/\rho)d} \quad (32.8)$$

where ρ is the scintillator mass density, μ/ρ is the scintillator total mass attenuation coefficient evaluated at the photon's energy, and d is the depth of the scintillator material, 4.4 cm for the NaI scintillator. Table 1 in Appendix C provides the total mass attenuation coefficients for outgoing photons from the target scattered into various angles.

Here's an example calculation: an incident ^{137}Cs photon (0.6616 MeV) is scattered by angle of 60° . Using Table 1 in Appendix C, the outgoing photon has 0.402 MeV, and at this energy the NaI $\mu/\rho = 0.117 \text{ cm}^2/\text{gm}$. Appendix C specifies $\rho = 3.67 \text{ gm}/\text{cm}^3$ for NaI. With these values and the scintillator depth of 4.4 cm, the probability of detection given by (32.8) is 0.85, so the

observed event rate should be divided by this probability to correct for the NaI detector efficiency.

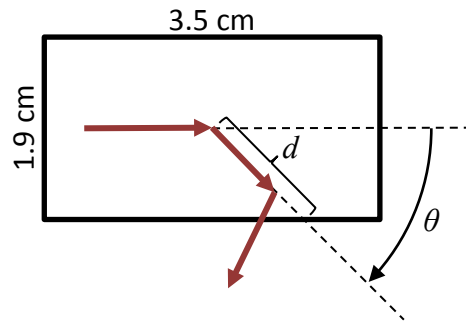
Correct the observed event rate at each θ by *dividing* by the NaI detection probability calculated using (32.8). If not using the values in Table 1 of Appendix C, then always use the *total* mass attenuation coefficient given by the chart for NaI in Appendix C.

You must use the total mass attenuation coefficient rather than, say, the coefficient for photoelectric absorption only. Except for relatively low-energy photons, the coefficient for Compton scattering in the NaI scintillator exceeds that for photoelectric absorption. The events which wind up in the full-energy peak in the NaI scintillator are usually due to multiple interaction events in the NaI scintillator: Compton scattering followed by photoelectric absorption of the outgoing photon. Similarly, multiple Compton scatterings also occur. You do not have an accurate way to model the probabilities of these multiple interaction scenarios, and, in particular, you cannot predict what fraction of the photons entering the NaI scintillator will contribute to its full-energy peak. You can only use the mass attenuation chart to estimate what fraction of the photons will undergo *some sort* of interaction or interactions in the NaI scintillator and thus be detected. Only the *total* mass attenuation coefficient is suitable for this purpose. This limitation will become important when deciding which coincidence events in the scintillator spectra should be counted and which should be discarded when calculating scattering rates.

Target scintillator self-absorption and multiple scattering corrections

A photon scattered by a target electron into the angle θ may suffer another scattering before exiting the target scintillator. In this case it will be lost from the set of photons scattered into the NaI scintillator positioned at θ . This occasional *self-absorption* by the target scintillator reduces the observed count rate, and you must correct for it: photons scattered a second time in the target scintillator away from the NaI angle θ do not result in coincidence detections because they do not enter the NaI scintillator. The geometry shown in Figure 14 illustrates the situation.

Figure 14: Self-absorption in the target scintillator occurs whenever an outgoing photon which would have reached the NaI scintillator positioned at angle θ is scattered again before it exits the target scintillator. To avoid this fate, the outgoing photon must (on average) travel the distance d without scattering. The view shown is from above the target scintillator.



To lowest order it is sufficient to consider an incident photon which is scattered near the center of the target scintillator volume. It must then traverse the distance d shown in Figure 14 before

exiting the target volume, which may be calculated from θ and the scintillator dimensions shown. The maximum value of d is 2.0 cm when θ is 28.5° (half the length of the diagonal of the rectangular target area shown in Figure 14). To calculate the probability that the photon exits along d without suffering an additional scattering we again turn to Table 1 in Appendix C, this time using the column for the plastic scintillator. This probability is given by equation (32.9).

$$P_T = e^{-\rho(\mu/\rho)d} \quad (32.9)$$

Example calculation: again consider a scattering angle of 60° . Using Table 1 in Appendix C, the outgoing photon has an energy of 0.402 MeV, and the plastic scintillator has a μ/ρ of $0.109 \text{ cm}^2/\text{gm}$ with a density $\rho = 1.18 \text{ gm}/\text{cm}^3$. At 60° , $d = (1.9 \text{ cm}/2)/\sin 60^\circ = 1.1 \text{ cm}$. The probability for the outgoing photon to avoid another scattering event is then calculated from equation (32.9) to be 0.87. The observed event rate should be divided by this probability to correct for target self-absorption.

Correct the observed event rate at each θ by *dividing* by the probability calculated using (32.9) for the distance d within the plastic target scintillator (Figure 14). Remember to use the *plastic* mass attenuation coefficient from Table 1 in Appendix C.

Mitigating the effect of multiple scatterings in the target

Conversely to the problem of target self-absorption, photons initially scattered into directions other than toward the NaI detector positioned at θ may be scattered again, this time so that they do exit the target toward the NaI detector. These multiply-scattered photons increase the observed rate, so events associated with them should not be counted.

The most straightforward way to recognize these extraneous events is by the energy they each deposit in the target scintillator. Multiple Compton scattering caused by a single incident photon can deposit a wide range of energies, both above and below that deposited by a single Compton scatter into outgoing direction θ . Consequently, these events can show up nearly anywhere on a scatter plot (refer to Figure 12 on page 15 and Figure 13 on page 16). The desired, single-Compton events for angle θ will all deposit the same energy in the target scintillator, namely $T(\theta) = k_0 - k'(\theta)$.

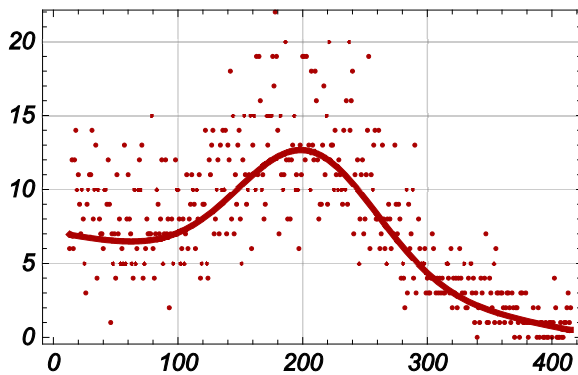
Consider again Figure 12 on page 15. Above the scatter plot in that figure is the corresponding target scintillator spectrum (histogram). This spectrum exhibits a broad Gaussian peak on a somewhat linearly-varying background. This peak is indeed associated with the desired, single-Compton events, including both full-energy and Compton-only interactions in the NaI scintillator. Thus the area of this Gaussian peak gives a count of the desired events (see the Prelab Problems).

Putting it all together

For each NaI detector angle θ in your data set, you must calculate your observed count rate/steradian, corrected for target self-absorption, NaI detector efficiency, and actual solid angle subtended. The Prelab Problems along with the example calculations outlined previously lead you through the steps. Your results will be a set of measured count rates/steradian (with uncertainties) vs. scattering angle θ (which also has an uncertainty). These rates should then be proportional to their corresponding $d\sigma/d\Omega|_{\theta}$ values. Quantitatively compare the variation in your measured data with scattering angle θ to that described by the Klein-Nishina theory, equation (32.4). You will find it useful to normalize both your measured rates and the Klein-Nishina cross-sections by dividing by their values at some common, convenient scattering angle, say 60° or 90° .

Prelab Problems

- Given that the fine structure constant $\alpha \equiv e^2/(4\pi\epsilon_0 \hbar c) \approx 1/137$, the electron's rest energy is 0.511 MeV, and $\hbar c = 1970 \text{ eV}\text{\AA}$, calculate an estimate of the classical electron radius r_e . What is then the electron's total cross section for Thomson scattering in *barns* (10^{-28} m^2)? What is its approximate total Klein-Nishina cross section for Compton scattering of the 0.6616 MeV ^{137}Cs γ -ray (consult *Appendix B*, Figure 22 on page 32–B–8)?
- The scattering data shown in Figure 12 on page 15 is for $\theta = 60^\circ$. Fitting a Gaussian on a linear background to the target scintillator count spectrum associated with this data gives the results shown below:



Gaussian fit results:

Peak height (y_{\max}): 8.75 ± 0.43 counts/chan

Standard deviation (sigma): 56.0 ± 3.2 chan

Given the peak height and standard deviation of the Gaussian, what is the total integrated count number it represents, with uncertainty (what is its integrated area)?

- Continuing the problem above, now correct the raw count data you have calculated for the expected NaI detector efficiency and for target self-absorption. What is the corrected count rate with uncertainty if the spectrum acquisition time was 480 seconds? If the separation of the scintillators was 40 cm, what is then the count rate/steradian?

APPENDIX A: TOTAL AND DIFFERENTIAL SCATTERING CROSS SECTIONS

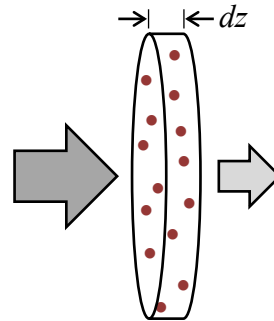
In this appendix we examine the concept of the *scattering cross section* between an incoming beam of particles interacting with a set of relatively motionless target particles (in our case photons and electrons). The *total cross section* describes the probability of any successful scattering of an incoming particle by a target, no matter what directions the scattered, outgoing particles may take, whereas the *differential cross section* characterizes the probability of the scattered particles assuming a particular outgoing set of directions. First we consider the total cross section, since it is in many ways the simpler concept.

Total scattering cross section and the mean free path

Consider the situation illustrated by Figure 15. A uniform beam of identical particles is incident on a very thin volume (infinitesimal thickness dz) containing an array of nearly motionless scattering targets (all identical to one another and with number density n). Some small fraction dP of the incoming particles will be scattered by the targets in the volume. Because the incident particles in the beam are all identical to each other, this fraction dP must be the probability that any particular incident particle will be scattered when passing through the target volume. Because the volume is of infinitesimal thickness, dP will be proportional to the total number of target particles in the volume encountered by the incident beam, which is in turn proportional to the target number density times the volume's thickness: ndz .¹² If we call the constant of proportionality σ (which must have dimensions of *area*), then we get

$$dP = \sigma n dz \quad (32.A.1)$$

Figure 15: A beam of identical particles is incident on a thin volume containing target particles. The volume has infinitesimal thickness dz , and the number density of the targets within the volume is n . Some of the incident particles are scattered by targets in the volume.



In the case of a finite volume thickness, assume that $N(z)$ particles in the incident beam have penetrated a distance z into the target volume without being scattered. Given the differential probability of scattering in (32.A.1), we expect that $N(z + dz) = (1 - dP)N(z) = (1 - \sigma ndz)N(z)$

¹² The expression ndz is called the differential *column density* of the target particles, because it describes the number of target particles along the depth of the volume per unit area of the volume's surface facing the incident beam. Clearly, the column density has dimensions of particles/area.

particles will avoid scattering for an additional distance dz . Thus $dN/dz = -\sigma nN(z)$. Integrating,

$$N(z) = N(0) \exp(-\sigma n z) \quad (32.A.2)$$

The number of incident particles avoiding a scattering event falls exponentially with distance into the volume containing the targets. The length

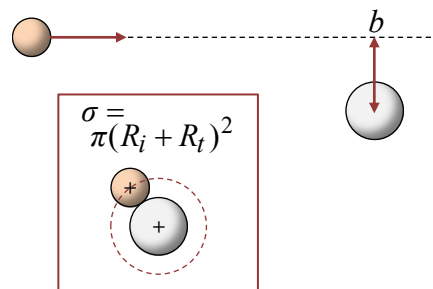
$$\lambda \equiv 1/(\sigma n) \quad (32.A.3)$$

is called the *mean free path* of the incident particles within this volume of stationary target particles.¹³

The area σ is called the *total cross section for scattering* of an incident particle by a single target particle. It can be interpreted as a small cross-sectional area centered on a target particle and oriented normal to the incident beam. If an incident particle's projected path would pass through this area around a target particle, then the incident particle is scattered out of the beam; otherwise it remains in the beam of unscattered incident particles. The numerical value of the total cross section σ will be determined by the physics of the interaction between the incident particle and the target. It will generally depend on the nature and strength of the forces between them as well as the relative kinetic energy of the particles as they approach.

Consider a simple example known as *hard sphere scattering*. Assume that the incident and target particles may be modeled as hard spheres of radii R_i and R_t , respectively. Further assume that the incident particle's projected, undeflected path would bring its center within distance b of the target particle's center (the distance b is called the *impact parameter*). Referring to Figure 16, if $b < R_i + R_t$, then the two particles will collide and therefore scatter; otherwise no scattering will take place. The resulting total cross section σ is therefore the area of a circle with radius $R_i + R_t$.

Figure 16: Hard sphere scattering: the incident and target particles are each modeled as spheres. The inset shows a view oriented along the path of the incident particle. If the impact parameter b is less than the sum of particles' radii (inset, dashed circle around the target's center), then the spheres will collide, and the particles will scatter. Thus σ , the total cross section for scattering, is given by the dashed circle's area.



¹³ The mean free path formula (32.A.3) is correct for incident particles moving at speeds much greater than those of the target particles (thus, the target particles are relatively stationary). If the particles are all identical and moving isotropically within some volume, as do the particles in an ideal gas, then the mean free path of any one particle of the gas is $1/\sqrt{2}$ of that given in (32.A.3).

Differential scattering cross section

The total cross section determines the probability of any sort of scattering caused by the interaction of the incident and target particles. The next level of detail is to determine the probabilities of scattering into various angles away from the incident particles' initial path. The direction of the path of an outgoing, scattered particle will be described using the spherical polar coordinate angles θ and φ (see Figure 17). The *differential solid angle* $d\Omega$ is then defined as a small area of a unit sphere (radius $\equiv 1$, area $\equiv 4\pi$) centered about an angular position (θ, φ) .

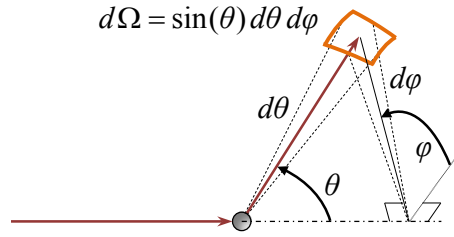


Figure 17: Differential solid angle $d\Omega$ into which an incoming particle may be scattered. Incident particles enter from the left and scatter from the target. We locate the angular position of the differential solid angle using spherical polar coordinates with polar angle θ and azimuthal angle φ as shown. The fraction of the incident particles which scatter into a $d\Omega$ centered at (θ, φ) is described by the *differential cross section* $d\sigma/d\Omega$.

The infinitesimal, nearly rectangular patch of the unit sphere defining $d\Omega$ in Figure 17 has sides of lengths $|d\theta|$ in the polar direction and $|\sin(\theta)d\varphi|$ in the azimuthal direction. The area of the patch is therefore:

$$d\Omega = |\sin(\theta) d\varphi d\theta| = |d\varphi d(\cos\theta)| \quad (32.A.4)$$

A tiny scattering cross section $d\sigma \geq 0$ is associated with scattering into the solid angle $d\Omega$ about the direction (θ, φ) . In the limit that $d\Omega$ becomes infinitesimal, $d\sigma$ is proportional to $d\Omega$. The derivative $d\sigma/d\Omega$ is called the *differential cross section* for scattering into (θ, φ) and is always taken to be nonnegative. Obviously, the total cross section σ should equal the integral of the differential cross section over the surface of the unit sphere:

$$\sigma = \oint_{4\pi} \frac{d\sigma}{d\Omega} d\Omega = \int_0^\pi \int_0^{2\pi} \frac{d\sigma}{d\Omega} \sin(\theta) d\varphi d\theta = \int_{-1}^1 \int_0^{2\pi} \frac{d\sigma}{d\Omega} d\varphi d(\cos\theta) \quad (32.A.5)$$

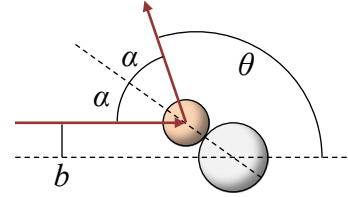
The final integral expression in (32.A.5) is often the most useful. If the scattering process is expected to have azimuthal symmetry (so that $d\sigma/d\Omega$ is independent of φ), then the integral over φ is equal to 2π , and

$$d\Omega = |2\pi d(\cos\theta)|$$

$$\frac{d\sigma}{d\Omega} = \frac{1}{2\pi} \frac{d\sigma}{d(\cos\theta)}; \quad \sigma = \int_{-1}^1 \frac{d\sigma}{d(\cos\theta)} d(\cos\theta) \quad (32.A.6)$$

Since increasing impact parameter b usually results in decreasing the expected polar scattering angle θ , we can usually assume that $d\sigma/d(\cos\theta) \geq 0$ in (32.A.6). In any case, the differential and total scattering cross sections should always be nonnegative. Returning to our previous example of hard sphere scattering, we assume that the spheres scatter elastically, and that the target particle is much more massive than the incident particle. We now calculate the differential cross section $d\sigma/d\Omega$ for scattering of the incident sphere into direction (θ, φ) . Consider the geometry of the scattering event depicted in Figure 18.

Figure 18: Geometry for elastic, hard sphere scattering used to calculate the differential cross section $d\sigma/d\Omega$. If the impact parameter $b < R_{tot}$, the sum of the spheres' radii, then scattering will occur into the angle $\theta = \pi - 2\alpha$.



Clearly, the scattering geometry is symmetric with regard to the azimuthal angle φ , so from the second of equations (32.A.6), we need only calculate how the scattering cross section varies with $\cos(\theta)$. Let the sum of the incident and target spheres' radii be $R_{tot} = R_i + R_t$. If the impact parameter b is greater than R_{tot} , then scattering will not occur; otherwise, assuming for simplicity's sake that the target is too massive to recoil with any significant velocity, the incident particle will recoil with the geometry shown, so that

$$\begin{aligned} \sin(\alpha) &= b/R_{tot} ; \quad \theta = \pi - 2\alpha \\ \therefore \cos(\theta) &= 2(b/R_{tot})^2 - 1 \end{aligned} \tag{32.A.7}$$

The final equation above is the result of a simple angle sum formula, or one could just use *Mathematica*® to derive it from the first two equations. Since the total integrated cross section for impact parameters less than b is πb^2 , we can use (32.A.6) and (32.A.7) to get

$$\frac{d\sigma}{d\Omega} = \frac{1}{2\pi} \frac{d\sigma/db}{d(\cos\theta)/db} = \frac{1}{4} R_{tot}^2 \tag{32.A.8}$$

So, interestingly, for elastic, hard sphere scattering from an immovable target, the differential scattering cross section is independent of the outgoing direction (θ, φ) .¹⁴ Multiplying this constant differential cross section by 4π steradians for the total solid angle Ω of the unit sphere gives our previous result for the total scattering cross section, $\sigma = \pi R_{tot}^2$, as expected.

¹⁴ This is also the correct result for the differential cross section for elastic, hard sphere scattering between any two particles, regardless of mass, if the particles' *center of momentum frame* is used to define the angles α and θ .

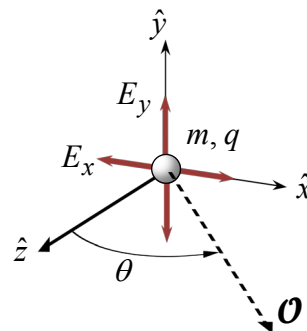
APPENDIX B: THOMSON SCATTERING AND ITS RELATIVISTIC COUNTERPART

Thomson scattering

Here we use classical theory to derive the scattering of electromagnetic radiation from an unbound (free), charged particle. The assumptions are that: (1) the wavelength of the radiation is much larger than the size of the particle; (2) net, average momentum transfer to the particle is negligible; and (3) the intensity of the radiation is low enough that the induced velocities of the particle are very small. This represents the low-energy limit of Compton scattering of a single photon and a free electron, and it was first derived by J. J. Thomson, the discoverer of the electron, in a book published in 1906; subsequently this theory has been known as *Thomson scattering*.¹⁵

Assume an unpolarized plane wave with intensity I_0 (radiant power per area) propagates in the \hat{z} direction and is incident on a small particle with mass m and charge q located at the origin. At any instant we can resolve the incident radiation into two linearly-polarized components: one with electric field oscillations along the \hat{x} direction, the other oscillating along the \hat{y} direction. On average, the intensity of each polarization component is $(1/2)I_0$, and their relative phases vary randomly. For the purposes of this analysis we will assume that each polarization electric field component E_x or E_y is a sinusoid with amplitude E_0 (Figure 19).

Figure 19: Geometry used to calculate classical, Thomson scattering of electromagnetic radiation by a charged particle. The incident wave propagates in the \hat{z} direction. Its oscillating field E_x or E_y (depending on the wave's polarization) then accelerates the particle (with mass m and charge q). The oscillating charge generates radiation in the direction of the observer \mathcal{O} , located in the x - y plane at an angle θ from \hat{z} .



Now we must consider how electromagnetic radiation is generated by the classical motion of a charged particle.¹⁶ Looking again at Figure 19, assume an observer sits at position \mathcal{O} in the x - z plane at a distance r from the particle. Let the unit vector $\hat{\mathbf{r}}$ point from \mathcal{O} toward the charge. What then would be the electric field $\vec{E}(t)$ and magnetic field $\vec{B}(t)$ produced at position \mathcal{O} by

¹⁵ Chapter XI, §161: “Theory of the secondary radiation,” in *Conduction of electricity through gasses*, J. J. Thomson, 1906. Joseph John Thomson won the 1906 Nobel Prize for his discovery of the electron in 1897. In 1912 he also discovered the existence of different isotopes of stable (nonradioactive) elements when he separated Neon-20 and Neon-22 using his invention of the mass spectrometer.

¹⁶ As with most of the ideas introduced in this course, Feynman explains it very clearly and elegantly. See his *Lectures on Physics*, Volume I chapter 28. Our presentation follows his (we refer to this text as *Feynman*).

the motion of the charge? *Feynman's* equations (28.3) and (28.4) give our equations (32.B.1) and (32.B.2):

$$\vec{E}(t) = \frac{-q}{4\pi\epsilon_0} \left[\frac{\hat{\mathbf{r}}(t_{ret})}{r^2(t_{ret})} + \frac{r(t_{ret})}{c} \frac{d}{dt} \left(\frac{\hat{\mathbf{r}}(t_{ret})}{r^2(t_{ret})} \right) + \frac{1}{c^2} \frac{d^2}{dt^2} \hat{\mathbf{r}}(t_{ret}) \right] \quad (32.B.1)$$

$$\vec{B}(t) = -\hat{\mathbf{r}}(t_{ret}) \times \frac{1}{c} \vec{E}(t) \quad (32.B.2)$$

where the *retarded time* t_{ret} refers to the time at which light (electromagnetic radiation) would have had to leave the particle in time to arrive at position \mathcal{O} at time t , that is $t_{ret} = t - r/c$, where r was the distance of the charge when the light would have been emitted: $r = r(t_{ret})$. The unit vector $\hat{\mathbf{r}}(t_{ret})$ points in the direction from \mathcal{O} to the charge at that earlier time, i.e. the *apparent* direction to the charge at time t . Note that all of the positions referred to in (32.B.1) and (32.B.2) must be evaluated at the retarded time t_{ret} . As explained in *Feynman*, the first two terms in the equation for $\vec{E}(t)$ simply represent the “effective” inverse square law Coulomb field produced at the observer’s position by the moving charge, and, falling off with distance as r^{-2} , do not contribute to the production of electromagnetic radiation by the charge; it is the final term, falling off with distance as r^{-1} , which interests us.

An oscillating electric field of amplitude E_0 will produce an oscillating acceleration of the particle at the same frequency and with amplitude $|d^2\xi/dt^2| = qE_0/m$, where ξ is the particle’s distance from the origin, which is assumed to be much smaller than the distance r of the observer at \mathcal{O} . Each polarization component E_x and E_y will induce a corresponding acceleration of the particle along its axis. From the geometry of Figure 19, at \mathcal{O} the amplitudes of the accelerations of the unit vector $\hat{\mathbf{r}}$ in the \hat{y} direction due to E_y and in the x - z plane due to E_x will be

$$\left| \frac{d^2}{dt^2} \hat{\mathbf{r}}_y \right| = \frac{1}{r} \left| \frac{d^2}{dt^2} \xi_y \right| = \frac{1}{r} \frac{qE_0}{m}; \quad \left| \frac{d^2}{dt^2} \hat{\mathbf{r}}_{x-z} \right| = |\cos(\theta)| \frac{1}{r} \left| \frac{d^2}{dt^2} \xi_x \right| = |\cos(\theta)| \frac{1}{r} \frac{qE_0}{m}$$

Using this result, the amplitudes of the corresponding electric and magnetic field components at \mathcal{O} are then given by (32.B.1) and (32.B.2). The intensity of the radiation is proportional to the sum of the squares of the electric field component amplitudes, so in terms of the intensities, $2E_0^2 \propto I_0$ and $E_y^2 + E_{x-z}^2 \propto I_s$, where the latter refers to the radiation from the particle observed at \mathcal{O} . Thus the scattered radiation intensity at \mathcal{O} is given by:

$$\frac{I_s}{I_0} = \left(\frac{1}{r} \right)^2 \left(\frac{q^2}{4\pi\epsilon_0 mc^2} \right)^2 \frac{1}{2} (1 + \cos^2 \theta) = \left(\frac{1}{r} \right)^2 \frac{r_e^2}{2} (1 + \cos^2 \theta) \quad (32.B.3)$$

As expected, the scattered radiation is at the same frequency as the incident radiation, and its intensity decreases as r^{-2} . In the final expression of (32.B.3), we assume that the particle is an

electron. The classical electron radius, r_e , provides a rough estimate of the “size” of an electron if one assumes that all of an electron’s rest energy mc^2 is due to the electrostatic potential energy of its charge:¹⁷

$$\frac{e^2}{4\pi\epsilon_0 r_e} = mc^2 \quad \rightarrow \quad r_e = \frac{e^2}{4\pi\epsilon_0 mc^2} \approx 2.818 \times 10^{-15} \text{ m}$$

Our first assumption upon which the derivation of (32.B.3) is based is that the wavelength of the radiation is much larger than the charged particle size, or $\gg r_e$. Because r_e is so tiny, this would only require that the incident photon’s energy $\ll 440 \text{ MeV}$, about 10^3 times the electron’s rest energy! In this highly relativistic regime, Thomson scattering certainly must be replaced by a quantum mechanical, relativistic theory. The actual limit for Thomson scattering is, of course, that the incident photon energy must be $\ll mc^2$, about 0.5 MeV for an electron.

To compare the Thomson result with the Klein-Nishina theory of Compton scattering, we must convert (32.B.3) into an expression for $d\sigma/d\Omega$, the differential cross section for Thomson scattering. First note, however, that we can derive the *total cross section* for Thomson scattering by integrating (32.B.3) over the unit sphere ($r \equiv 1$),¹⁸ giving the ratio of the total scattered power to the incident intensity:

$$\text{Thomson:} \quad \sigma = \oint\!\!\!\oint_{4\pi} \frac{I_s(r \equiv 1)}{I_0} d\Omega = \pi r_e^2 \int_{-1}^1 (1 + \cos^2 \theta) d(\cos \theta) = \frac{8\pi}{3} r_e^2 \quad (32.B.4)$$

This result for the total cross section for scattering of electromagnetic radiation by a free electron was derived by J. J. Thomson in his 1906 book cited earlier (footnote 15).

To get the differential cross section is easy: $d\sigma = (d\sigma/d\Omega) d\Omega$, and from our integration (32.B.4), $(d\sigma/d\Omega)$ must be the integrand of the first integral. Therefore,

$$\text{Thomson:} \quad \frac{d\sigma}{d\Omega} = \frac{I_s(r \equiv 1)}{I_0} = \frac{r_e^2}{2} (1 + \cos^2 \theta) = \frac{r_e^2}{2} (2 - \sin^2 \theta) \quad (32.B.5)$$

The final expression in (32.B.5) is useful for comparison to the Klein-Nishina theory. Remember that this result is for an *unpolarized* radiation source (equal amounts of vertical and horizontal linear polarizations, averaged over all possible phase relationships between them). In this case the scattering cross section is independent of the azimuthal scattering angle ϕ .

¹⁷ NIST listing of the currently-accepted value: <https://physics.nist.gov/cgi-bin/cuu/Value?re>.

¹⁸ Equivalently, we could integrate the scattered intensity over the surface area of a sphere with radius r centered on the source. In terms of the differential solid angle, the differential area of the sphere’s surface is $da = r^2 d\Omega$. The results for the total and differential cross sections will be the same as (32.B.4) and (32.B.5).

Relativistic, single photon scattering

Now we extend our previous result in the most straightforward way possible to include the scattering of a high-energy photon by a charged particle (so we are considering a *very* simplistic version of *quantum electrodynamics*). Such an event may transfer significant amounts of linear momentum and kinetic energy to the target, so that the target recoils and the scattered (outgoing) photon will have less energy (and a lower frequency). In the photon-target center of momentum (CM) frame, however, the incident and scattered photons have the same energy, because the scattering is assumed to be elastic (Figure 20).

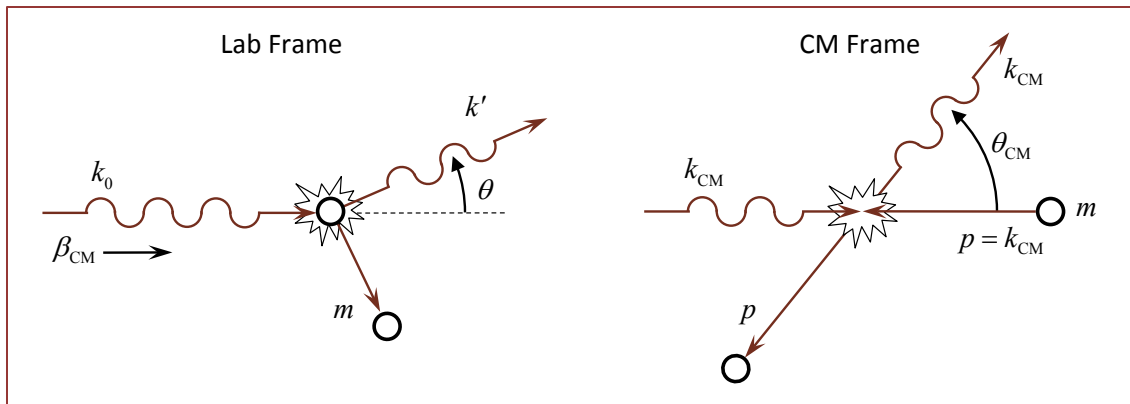


Figure 20: Geometry illustrating photon-charge scattering in the lab frame and the center of momentum (CM) frame. In the lab frame the incoming photon energy (and momentum) is k_0 , and its scattered energy is k' . The scattering is elastic, so in the CM frame incident and outgoing particle energies are the same, and the photon and target particle momenta are always oppositely directed with equal magnitudes. The CM frame moves with velocity β_{CM} relative to the lab frame.

Because in the CM frame the incoming and outgoing frequencies of the light are equal, we assume that we can use the completely classical Thomson scattering results of the previous section to describe the scattering interaction in that frame. In particular, we assume that an incident photon stream, described using the CM frame kinematics of Figure 20, generates an oscillating electric field on an array of target particles. The Thomson cross section derivation of the previous section then properly describes the induced to incident intensity ratios in the CM frame. Our big assumption is that these classically-derived intensity ratios, when interpreted as the differential cross section $d\sigma/d\Omega$ as a function of scattering angle, can be used to describe the quantum mechanical, single photon to single target particle scattering probabilities in the CM frame. This hybrid approach is therefore called a *semi-classical* analysis: it only becomes quantum because we interpret these classical, intensity-based cross sections as describing photon scattering event probabilities.

One must be careful to properly transform the relevant quantities between the lab and CM frames. Because an incoming photon as observed in the lab frame may have a kinetic energy comparable to or exceeding the target particle's rest energy, we must use special relativity. In order to properly follow the math in this section, the reader should review the relevant sections

of General Appendix A: *Relativistic Kinematics*,¹⁹ because we will make use of several of the results found there. As in the theory section of the main text, we choose units such that $c \equiv 1$ and $\hbar \equiv 1$. Thus, for example, both a photon's kinetic energy and its momentum may be represented by its wave number k , an electron's mass m is represented by its rest energy, 0.511 MeV, and the speed of the CM frame relative to the lab frame is expressed using $\beta \equiv v/c$. In the lab frame the incident photon energy is designated by k_0 and the scattered photon by k' . The lab frame scattering angle is θ . The CM frame photon energy is designated by k_{CM} (both incident and scattered) and the corresponding scattering angle is θ_{CM} (see Figure 20).

To use the Thomson results, we must calculate the incident radiation intensity in the CM frame, I_{CM} . In the lab frame the incident intensity I_0 may be interpreted as the product of the photon energy k_0 and the photon flux n_0 (photons per time per area): $I_0 = n_0 k_0$. Because the CM frame is moving relative to the lab frame, both the incident photon frequency and the photon flux will be Doppler-shifted when transformed to the CM frame. Using General Appendix A results (A-13) and (A-11),

$$\text{CM speed:} \quad \beta = \frac{1}{1 + m/k_0} \quad (32.B.6)$$

$$\begin{aligned} \text{CM Doppler shift:} \quad \frac{k_{\text{CM}}}{k_0} &= \frac{n_{\text{CM}}}{n_0} = \gamma(1 - \beta) = \sqrt{\frac{1 - \beta}{1 + \beta}} \\ \therefore \frac{I_{\text{CM}}}{I_0} &= \frac{n_{\text{CM}} k_{\text{CM}}}{n_0 k_0} = \frac{1 - \beta}{1 + \beta} \end{aligned} \quad (32.B.7)$$

Thomson cross sections calculated in the CM frame, which were derived using incident and scattered intensities, must be reduced by the relative intensity factor (32.B.7) when referred back to the lab frame to correct for the Doppler shift:

$$I_0 \sigma = I_{\text{CM}} \sigma_{\text{CM}} \rightarrow \frac{d\sigma}{d\sigma_{\text{CM}}} = \frac{I_{\text{CM}}}{I_0} \quad (32.B.8)$$

We will need one more relationship derivable from (32.B.6) and (32.B.7):

$$\frac{I_0}{I_{\text{CM}}} = \frac{1 + \beta}{1 - \beta} = \frac{1/\beta + 1}{1/\beta - 1} = \frac{2 + m/k_0}{m/k_0} = 1 + 2k_0/m \quad (32.B.9)$$

Next we must find a further relationship between the scattering cross sections in the two frames: how a differential solid angle in the CM frame, $d\Omega_{\text{CM}}$, is related to its corresponding differential solid angle in the lab frame, $d\Omega$. Because of *relativistic beaming* due to the motion of the CM frame (really just velocity addition), a photon scattered into angle θ_{CM} in the CM frame will be

¹⁹ http://www.sophphx.caltech.edu/Physics_7/General_Appendix_A.pdf

observed in the lab frame to scatter into a different, smaller angle θ (Figure 20); the azimuthal angle φ is unaffected by the Lorentz transformation. From (32.A.4),

$$\frac{d\Omega_{\text{CM}}}{d\Omega} = \frac{\cancel{d\varphi_{\text{CM}}} \frac{d(\cos\theta_{\text{CM}})}{d\varphi}}{\cancel{d\varphi}} \underset{=1}{=} \frac{d(\cos\theta_{\text{CM}})}{d(\cos\theta)}$$

Transforming an outgoing photon's 4-velocity with angle θ in the lab frame to angle θ_{CM} in the CM frame, the corresponding cosines are related by the first of equations (A-12) in General Appendix A (that equation's θ' will refer to our scattering angle θ in the lab frame). Thus

$$\frac{d\Omega_{\text{CM}}}{d\Omega} = \frac{d(\cos\theta_{\text{CM}})}{d(\cos\theta)} = \frac{d}{d(\cos\theta)} \left(\frac{\cos\theta - \beta}{1 - \beta \cos\theta} \right) = \frac{1 - \beta^2}{(1 - \beta \cos\theta)^2}$$

Using equation (32.B.6) for β and rearranging (*Mathematica*® is convenient for this purpose):

$$\frac{d\Omega_{\text{CM}}}{d\Omega} = \frac{1 - \beta^2}{(1 - \beta \cos\theta)^2} = \frac{1 + 2k_0/m}{[1 + (k_0/m)(1 - \cos\theta)]^2}$$

The numerator of the final expression above looks suspiciously similar to (32.B.9), and its denominator reminds one of the kinematic Compton scattering formula (32.1). Substituting:

$$\text{CM vs. lab solid angles:} \quad \frac{d\Omega_{\text{CM}}}{d\Omega} = \frac{1 + \beta}{1 - \beta} \left(\frac{k'}{k_0} \right)^2 \quad (32.B.10)$$

Now we can put it all together, using (32.B.8), (32.B.7), (32.B.10), and (32.B.5):

$$\begin{aligned} \frac{d\sigma}{d\Omega} &= \frac{d\sigma}{d\sigma_{\text{CM}}} \frac{d\sigma_{\text{CM}}}{d\Omega} = \frac{d\sigma}{d\sigma_{\text{CM}}} \frac{d\Omega_{\text{CM}}}{d\Omega} \frac{d\sigma_{\text{CM}}}{d\Omega_{\text{CM}}} \\ &= \left(\frac{1 - \beta}{1 + \beta} \right) \left(\frac{1 + \beta}{1 - \beta} \right) \left(\frac{k'}{k_0} \right)^2 \frac{r_e^2}{2} (1 + \cos^2 \theta) \end{aligned}$$

$$\text{"Spinless" electron scattering:} \quad \boxed{\frac{d\sigma}{d\Omega} = \frac{r_e^2}{2} \left(\frac{k'}{k_0} \right)^2 (1 + \cos^2 \theta)} \quad (32.B.11)$$

This, then, is our differential cross section for scattering high-energy photons by electrons, which turns out to agree with a much more interesting 1926 derivation by Dirac using his newly-developed ideas for relativistic quantum mechanics.²⁰ Dirac also used a semi-classical method to describe the interactions between the electron and both the incident and induced electromagnetic

²⁰ P. A. M. Dirac, "Relativity quantum mechanics with an application to Compton scattering," *Proc. Royal Soc. A*, **111**, 405 (1926): <http://rspa.royalsocietypublishing.org/content/111/758/405.article-info>. At that time Dirac was still a graduate student at Cambridge; he received his Ph.D. the same month his paper was published. See also §14.8 of J. D. Jackson, *Classical Electrodynamics* (3rd ed.), John Wiley & Sons (1998).

fields. Because $k' < k_0$ except when $\theta = 0$, the differential cross section falls rapidly below the classical, Thomson value as θ increases.

Compton made an heroic attempt in his 1923 paper (footnote 8) to derive the differential scattering cross section. He used a more complicated set of relativistic manipulations compared to those leading to (32.B.11), and his result differs from ours (and Dirac's) except at angles of 0° and 180° . Figure 21 compares the relative intensities predicted by equation (32.B.11)²¹ and by Compton's calculations of the scattered radiation from what at the time was thought to be a 0.56 MeV source (0.022 Å); also included are the measured scattering data from his 1923 paper. Dirac noted that scaling Compton's measured data by a factor of 4/3 brought it into reasonable agreement with Dirac's predicted scattering behavior.²²

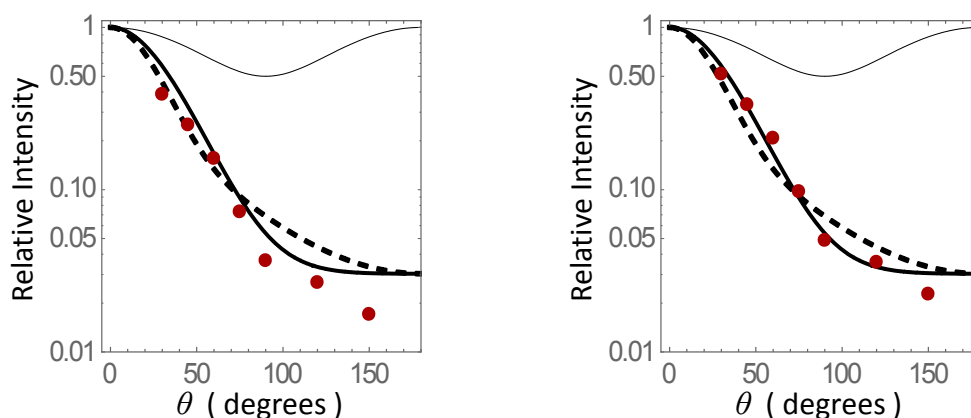


Figure 21: Comparison of A. Compton's 1923 calculation of the scattering cross section (dashed line) to that of equation (32.B.11) for 0.56 MeV incident photons. Thomson's classical theory is also included for reference (thin black line). Note that the intensity is plotted using a log scale. Left graph: comparison with Compton's measured intensity data (red circles). Right graph: Compton's measured data scaled by a factor of 4/3, as suggested by Dirac, brings it into good agreement with that predicted by (32.B.11) (but see footnote 22).

Electron spin, pair production

The previous derivation left out one small but important detail: the electron has a magnetic moment generated by its intrinsic angular momentum. Its magnetic dipole interacts with an

²¹ Equation (32.B.11) gives the probability of photon scattering into various angles. To convert to a ratio of scattered to incident intensity, it must be multiplied by the relative photon energy, adding another factor of k'/k_0 . This was actually the form of (32.B.11) presented by Dirac in 1926. Dirac's paper compared his theory to that calculated by Compton and to the data Compton reported in his 1923 paper. Figure 21 shows our version of that comparison.

²² Klein and Nishina (discussed in the next section) disputed the claimed characteristics of the radiation Compton used for his measured results. In particular, they doubted that the incident radiation had a wavelength of 0.022 Å; they thought that it might have had a shorter wavelength. They were probably right: Compton called his source "Radium C," which we now know to be ^{214}Bi , whose dominant γ -ray emission is 0.61 MeV, and not 0.56 MeV (with wavelength 0.022 Å).

incident photon’s oscillating magnetic field to create an additional scattering mechanism, so the result (32.B.11) is incomplete (it would actually be correct for a charged but spinless elementary particle, if only there were such a thing!²³). The electron’s spin 1/2 is a purely quantum mechanical property which can’t be accommodated using the approach of the previous section (it might be included using some “fast and loose” hand-waving, which we’ll forego).

When properly calculated using Dirac’s theory, as did physicists Oskar Klein and Yoshio Nishina,²⁴ equation (32.B.11) is modified by the inclusion of an extra term, which, as mentioned in the main text, becomes equation (32.4):

$$\frac{d\sigma}{d\Omega} = \frac{r_e^2}{2} \left(\frac{k'}{k_0}\right)^2 (2 - \sin^2 \theta) \rightarrow \frac{r_e^2}{2} \left(\frac{k'}{k_0}\right)^2 \left(2 - \sin^2 \theta + \frac{(k_0 - k')^2}{k_0 k'}\right) = \boxed{\frac{r_e^2}{2} \left(\frac{k'}{k_0}\right)^2 \left(\frac{k'}{k_0} + \frac{k_0}{k'} - \sin^2 \theta\right)}$$

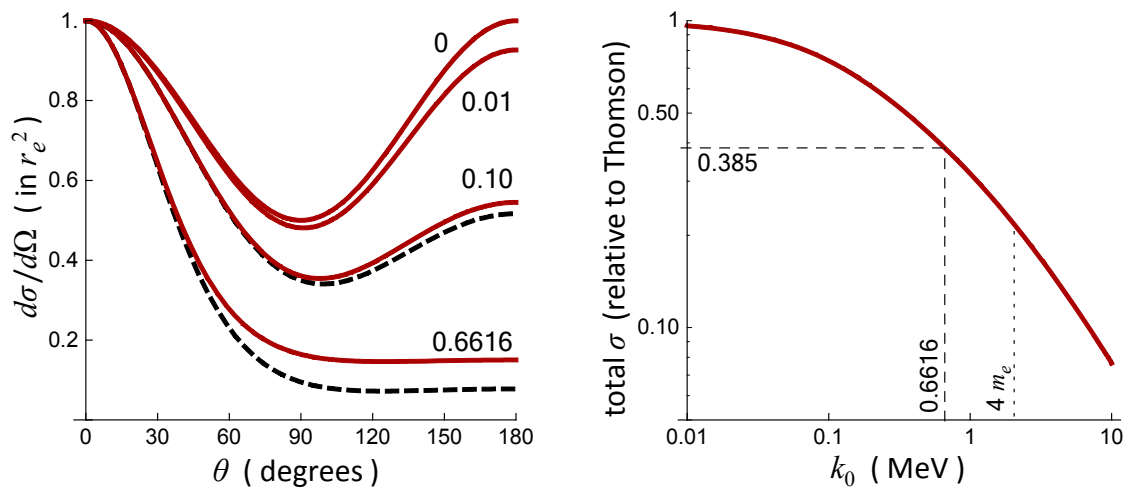


Figure 22: Scattering cross section comparisons. Left: Klein-Nishina (red) and equation (32.B.11) (dashed) differential cross sections vs. scattering angle for various incident photon energies (in MeV). Right: Klein-Nishina total scattering cross section vs. incident photon energy. The vertical dotted line is at the threshold energy for electron-positron pair production (see text).

This *Klein-Nishina differential cross section* increases relative to (32.B.11) for large k_0 at large scattering angles. They are compared in Figure 22. Also shown in that figure is a plot of the integrated, total cross section for Compton scattering as a function of incident photon energy (using the Klein-Nishina formula). For low photon energies the total scattering cross section

²³ Mesons such as the charged pions might seem to qualify, but they are not elementary particles, being bound quark-antiquark pairs. Their composite nature spoils the simple formula (32.B.11).

²⁴ The history and methodology of their derivation is examined in detail by Yuji Yazaki, “How the Klein–Nishina formula was derived: Based on the Sangokan Nishina Source Materials,” *Proc. Japan Acad. B*, **93**, 399 (2017): <https://doi.org/10.2183/pjab.93.025>.

approaches the Thomson value of $(8\pi/3) r_e^2$. Decreasing with increasing energy, the total cross section for 10 MeV photons is approximately 10% of its value for 0.1 MeV photons.

For incident photons with energies much higher than 1 MeV another interaction competes with Compton scattering: *pair production*. If an incident photon has an energy higher than 4 times the electron rest energy, it can undergo an *inelastic* collision with an electron, using the energy of the collision to create an electron-positron particle pair to accompany the electron (the energy threshold for pair production is given by General Appendix A, equation (A-17); see footnote 19). Although in a solid material (such as a scintillator crystal) pair production is much more likely to be due to a photon's interaction with an atomic nucleus (because of its greater electric charge and much greater mass), it can still occur during a collision with an electron, especially at very high photon energies (100's of MeV). In these cases simple Compton scattering is quite unlikely. At still higher energies, heavier particle-antiparticle pairs may be created.

APPENDIX C: MASS ATTENUATION COEFFICIENTS

Summary Data

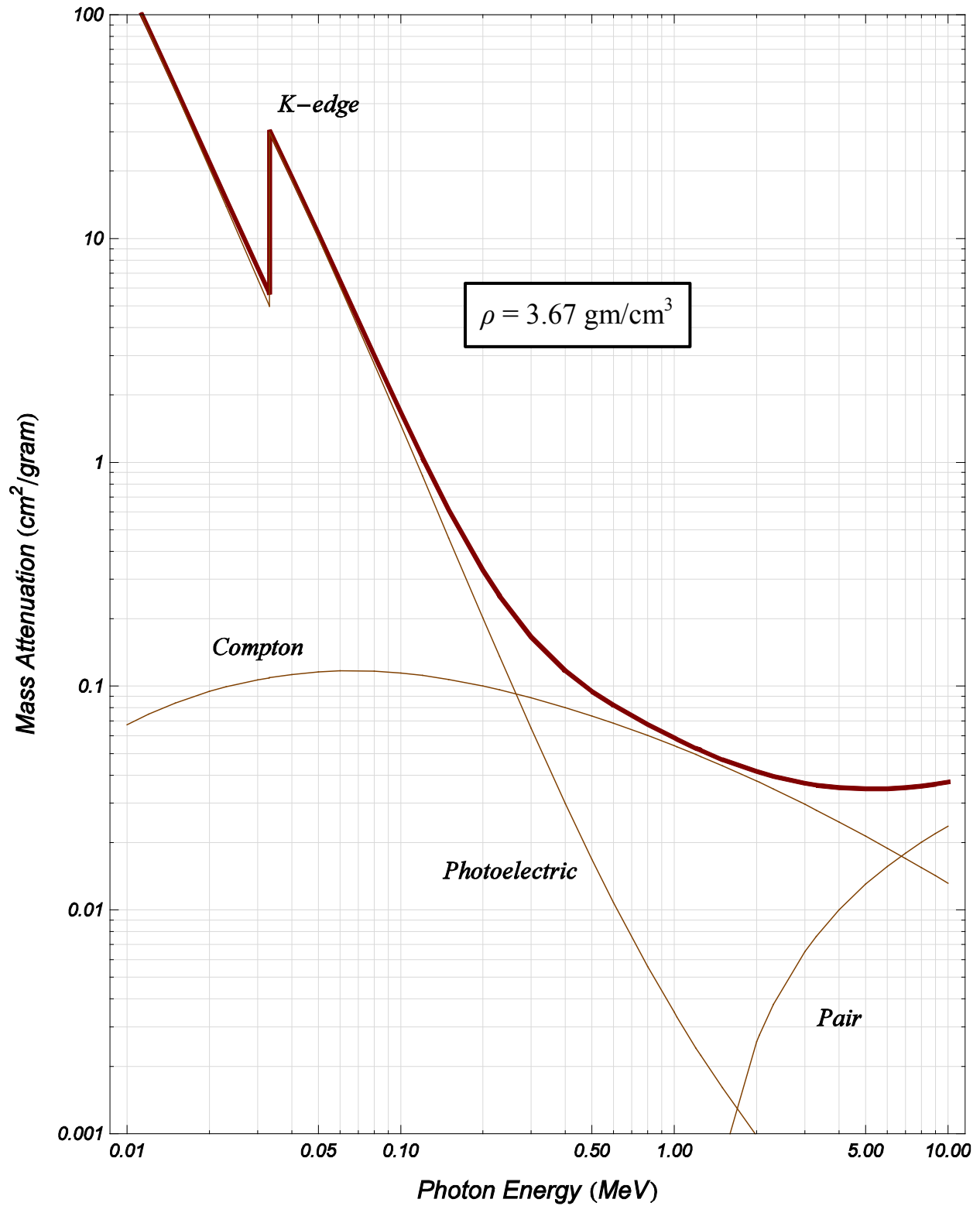
Compton scattering an incident ^{137}Cs photon (0.6616 MeV) through the angles specified in the first column of the following table results in an outgoing photon with the listed energy, as determined using the Compton scattering formula, equation (32.1). Using this energy value, the total mass attenuation coefficients for the NaI and Plastic scintillators are determined from the mass attenuation coefficient charts on the next pages of this appendix.

Table 1
Total Mass Attenuation Coefficients

θ (deg)	Energy (MeV)	NaI μ/ρ (cm^2/gm)	CH ₂ μ/ρ (cm^2/gm)
20	0.614	0.081	0.091
30	0.564	0.086	0.095
40	0.508	0.094	0.099
50	0.452	0.104	0.104
60	0.402	0.117	0.109
70	0.357	0.133	0.114
80	0.320	0.152	0.119
90	0.288	0.175	0.123
100	0.263	0.202	0.128
110	0.242	0.232	0.132
120	0.225	0.263	0.135
130	0.212	0.295	0.138
140	0.201	0.324	0.140
150	0.194	0.350	0.142

The density of Sodium Iodide (NaI) is $\rho = 3.67 \text{ gm/cm}^3$. The density of plastic (CH₂) is $\rho = 1.18 \text{ gm/cm}^3$.

Refer to Appendix B of the Experiments 30a and 30b notes for details on how to interpret the charts: http://www.sophphx.caltech.edu/Physics_7/Experiment_30a_and_30b.pdf.

Charts**Sodium Iodide (NaI)**

Plastic (CH₂)